Inorg. Chem. **2007**, *46*, 10564–10577

Cu^{2+} Colorimetric Sensing and Fluorescence Enhancement and Hg^{2+} Fluorescence Diminution in "Scorpionate"-like Tetrathienyl-Substituted Boron–Dipyrrins

Shin Hei Choi,[†] Keliang Pang,[‡] Kibong Kim,[†] and David G. Churchill*,[†]

Department of Chemistry and School of Molecular Science (BK 21), KAIST, Daejeon 305-701, Korea, and Department of Chemistry, Columbia University, 3000 Broadway, New York, New York 10027

Received June 5, 2007

Four novel tetrathienyl-substituted boron–dipyrrin-type (BODIPY-type) complexes, 3-(R′)-4,4-di(R′)-8-R-4-bora-3a,4a-diaza-s-indacene (**4a**, R = 2-T, R′ = 2-T; **4b**, R = 3-T, R′ = 2-T; **5a**, R = 2-T, R′ = 3-T; **5b**, R = 3-T, R′ = 3-T; T = thienyl) have been prepared and fully characterized to explore patterns of stoichiometric M^{n+} recognition in solution. Treatment of the respective parent BF_2 dipyrrin with 2- or 3-thienyllithium gave the unexpected asymmetric tetrathienyl-substituted products in 8.5–35% yield. Compounds **4a** and **4b** bear a neutral "scorpionate"-like [SSS] tridentate binding pocket. Extensive NMR and UV–vis spectroscopic studies were performed on **4a**–**5b**; **5a**, **4b**, and **5b** were structurally characterized. The Φ_F values for **4a**–**5b** all decrease compared to the BF_2-containing parent molecules (0.00058, 0.012, 0.00090, and 0.0051, respectively), with $\lambda_{abs,max}$ values (ϵ, M^{-1} cm^{-1}) of 563 (44 000), 553 (29 000), 539 (33 000), and 531 (44 000) nm, respectively, and Stokes' shifts of 25–36 nm. Upon treatment with metal ion (Ca^{2+}, Cs^{+}, Mn^{2+}, Co^{2+}, Cu^{2+}, Ag^{+}, Zn^{2+}, Cd^{2+}, Hg^{2+}, Pb^{2+}) perchlorate salts, the solution of **4b** undergoes rapid pink-to-clear switch-off behavior upon Cu^{2+} addition (10 μM scale) with smaller effects seen for **4a.** Further, there were 2- to 19-fold Cu^{2+} fluorescence enhancements for these ligands. Cu^{2+}– and Hg^{2+}–L (L = **4a**–**5b**) binding was modeled, and response patterns for M^{n+}–L 1:1 molar solutions upon Cu^{2+} addition were measured. Upon treatment with Hg^{2+}, all ligand solutions show a significant fluorescence decrease accompanied by minor absorption increases. The UV–vis spectroscopic detection limit for Cu^{2+} and Hg^{2+} is ∼270 ppb and ∼1.7 ppm, respectively; the naked eye detection limit for Cu^{2+} with **4b** (1.0×10^{-5} M) is ∼23 μM. DFT calculations gave HOMO–LUMO gaps of 478 (**4a**), 462 (**4b**), 448 (**5a**), and 442 nm (**5b**). Molecular orbital diagrams for **4a**–**5b** revealed that the HOMO and LUMO electron density is distributed onto the 3-position-thienyl group and to a lesser degree the $B(thienyl)_2$ moiety.

1. Introduction

Investigations into well-defined small-molecule receptors that give rise to visible or luminescent changes upon interaction with metal ions (ionophores) continue unabated as new chemosensing platforms are synthesized and explored.[1–4] In particular, sensors, switches, and dosimeters have recently been reported for the cupric (Cu^{2+})[5–18] and mercuric ions (Hg^{2+})[13,19–30] with extremely varied constituent fragments, stemming from small parent molecules such as anthracene, pyrene, cyclodextrin, calyx[4]arene, fluorescein, quinoline, rhodamine, azulene, pyridine, thiazole, thiadiazole, thiophene, cyclam, BODIPY, ferrocene, carbohydrates, and peptides. Sensing of Cu^{2+} is interesting in that cupric ion is found widely in nature and plays various roles in living systems as a trace element that features in the active sites of some key enzymes. Hg^{2+} is also found commonly in nature as cinnebar but used in industry; thus, Hg and its ions loom as anthropogenic environmental contaminants in aquifers and soils able to be transformed into highly neurotoxic methyl

* To whom correspondence should be addressed. E-mail: dchurchill@kaist.ac.kr.
† KAIST.
‡ Columbia University.

(1) *Molecular Fluorescence: Principles and Applications*; Valeur, B., Ed.; Wiley-VCH: Weinheim, Germany, 2002.
(2) *Molecular Switches*; Feringa, B. L. Ed.; Wiley-VCH: Weinheim, 2001.
(3) Haugland, R. P. *Handbook of Fluorescent Probes and Research Chemical*, 9th ed.; Molecular Probes, Inc.: Eugene, OR, 2002.

10.1021/ic701101j CCC: $37.00
Published on Web 11/09/2007

mercury. Both cations are interesting subjects of assays in the exploration of new ionophores.

Boron−dipyrrin-type (bora−di- and bora−triazaindacene) frameworks have featured in Cu^{2+} and Hg^{2+} recognition[18,20,28,30,31] but usually involve "tried and true ligation" themes: e.g., pyridyl and "crown" moieties. Boron−dipyrrin derivatives have been difficult to prepare in large quantities, but routes to achieve satisfactory yields of 5-substituted BF_2−dipyrrins are possible through reports that ease the preparation of the requisite 5-substituted dipyrromethanes.[32,33] Interest in 5-substituted systems (aka, 8-substituted, see Figure 1) has become keen since a recent report involving profound photodynamic property changes that occur upon simple 8-position modification (i.e., phenyl ($\Phi_F = \sim 0.06$) and the *o*-tolyl ($\Phi_F = \sim 0.9$)) in BF_2−dipyrrin chemistry was published.[34] This notion of extreme sensitivity regarding 8-aryl substitution led us to prepare closely related thienyl derivatives in exploring potential probes for hydrodesulfurization catalysts[35] with the idea being that desulfurization or sulfoxidation events would drastically change said properties.[36] We have been exploring, *generally*, how thienyl substituents featured in ligation or thiophene cores serve as chelation unit frameworks[37,38] and now set out further to explore receptor sites bearing *multiple* thienyl groups. Thienyl groups involve weak M^{n+}−$S_{thienyl}$ binding and do not take part in hydrogen bonding different from the common carboxylate or amino groups. Thus, by considering that difluoroboryl fluorines can be replaced by aryl moieties, as reported by Ziessel and co-workers,[39,40] we aimed to prepare multiple thienyl bearing boron−dipyrrins derivatives, isomers (2 and 3 and mixed systems)[41] where patterns in ligand substitution may lead to patterns in M^{n+} recognition. Herein is a careful synthetic, spectroscopic, spectrometric, structural, and theoretical study focused on stoichiometric M^{n+} recognition using multi-thienyl-substituted boron−dipyrrins.

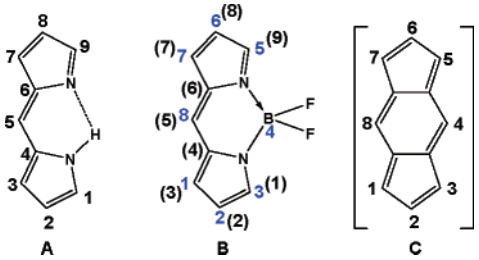

Figure 1. Numbering conventions: (A) dipyrrin (aka, dipyrromethene), (B) 4-bora-3a,4a-diaza-s-indacene or BF_2-dipyrrin (dipyrrin numbering in parentheses), and (C) s-indacene.

2. Experimental Section

General Considerations. All chemicals (e.g., pyrrole, 2-thiophene carboxaldehyde, 3-thiophene carboxaldehyde, CH_2Cl_2, hexane, and M^{n+} perchlorates) used herein were of analytical grade and used as received from commercial suppliers (Aldrich and Junsei chemical companies). ***Caution!*** *Perchlorate salts are known chemical explosion hazards.*[42] The synthetic details for the preparation of 5-(thienyl)dipyrromethanes and difluoroboryl-thienyl dipyrrins have been reported previously.[36,43] Plates for (i) preparative thin layer

(4) de Silva, A. P.; Gunaratne, H. Q. N.; Gunnlaugsson, T.; Huxley, A. J. M.; McCoy, C. P.; Rademacher, J. T.; Rice, T. E. *Chem. Rev.* **1997**, *97*, 1515−1566.
(5) Kramer, R. *Angew. Chem., Int. Ed. Engl.* **1998**, *37*, 772−773.
(6) Liu, J. M.; Zheng, Q. Y.; Yang, J. L.; Chen, C. F.; Huang, Z. T. *Tetrahedron Lett.* **2002**, *43*, 9209−9212.
(7) Torrado, A.; Walkup, G. K.; Imperiali, B. *J. Am. Chem. Soc.* **1998**, *120*, 609−610.
(8) Corradini, R.; Dossena, A.; Galaverna, G.; Marchelli, R.; Panagia, A.; Sartor, G. *J. Org. Chem.* **1997**, *62*, 6283−6289.
(9) Yang, R. H.; Zhang, Y.; Li, K. A.; Liu, F.; Chan, W. H. *Anal. Chim. Acta* **2004**, *525*, 97−103.
(10) Boiocchi, M.; Fabbrizzi, L.; Licchelli, M.; Sacchi, D.; Vazquez, M.; Zampa, C. *Chem. Commun.* **2003**, 1812−1813.
(11) Singhal, N. K.; Ramanujam, B.; Mariappanadar, V.; Rao, C. P. *Org. Lett.* **2006**, *8*, 3525−3528.
(12) Martinez, R.; Zapata, F.; Caballero, A.; Espinosa, A.; Tarraga, A.; Molina, P. *Org. Lett.* **2006**, *8*, 3235−3238.
(13) (a) Martinez, R.; Espinosa, A.; Tarraga, A.; Molina, P. *Org. Lett.* **2005**, *7*, 5869−5872. (b) Guo, Z.; Zhu, W.; Shen, L.; Tian, H. *Angew. Chem., Int. Ed.* **2007**, *46*, 5549−5553.
(14) Wen, Z. C.; Yang, R.; He, H.; Jiang, Y. B. *Chem. Commun.* **2006**, 106−108.
(15) Mokhir, A.; Kiel, A.; Herten, D. P.; Kraemer, R. *Inorg. Chem.* **2005**, *44*, 5661−5666.
(16) Zhou, L. L.; Sun, H.; Zhang, X. H.; Wu, S. K. *Spectrochim. Acta, Part A* **2005**, *61*, 61−65.
(17) Mitchell, K. A.; Brown, R. G.; Yuan, D. W.; Chang, S. C.; Utecht, R. E.; Lewis, D. E. *J. Photochem. Photobiol., A* **1998**, *115*, 157−161.
(18) Qi, X.; Jun, E. J.; Xu, L.; Kim, S. J.; Hong, J. S. J.; Yoon, Y. J.; Yoon, J. Y. *J. Org. Chem.* **2006**, *71*, 2881−2884.
(19) Yang, Y. K.; Yook, K. J.; Tae, J. *J. Am. Chem. Soc.* **2005**, *127*, 16760−16761.
(20) Rurack, K.; Kollmannsberger, M.; Resch-Genger, U.; Daub, J. *J. Am. Chem. Soc.* **2000**, *122*, 968−969.
(21) Wu, Z. K.; Zhang, Y. F.; Ma, J. S.; Yang, G. Q. *Inorg. Chem.* **2006**, *45*, 3140−3142.
(22) Caballero, A.; Lloveras, V.; Curiel, D.; Tarraga, A.; Espinosa, A.; Garcia, R.; Vidal-Gancedo, J.; Rovira, C.; Wurst, K.; Molina, P.; Veciana, J. *Inorg. Chem.* **2007**, *46*, 825−838.
(23) Coronado, E.; Galan-Mascaros, J. R.; Marti-Gastaldo, C.; Palomares, E.; Durrant, J. R.; Vilar, R.; Gratzel, M.; Nazeeruddin, M. K. *J. Am. Chem. Soc.* **2005**, *127*, 12351−12356.
(24) Wakabayashi, S.; Kato, Y.; Mochizuki, K.; Suzuki, R.; Matsumoto, M.; Sugihara, Y.; Shimizu, M. *J. Org. Chem.* **2007**, *72*, 744−749.
(25) Song, K. C.; Kim, J. S.; Park, S. M.; Chung, K. C.; Ahn, S.; Chang, S. K. *Org. Lett.* **2006**, *8*, 3413−3416.
(26) Hennrich, G.; Sonnenschein, H.; Resch-Genger, U. *J. Am. Chem. Soc.* **1999**, *121*, 5073−5074.
(27) Ho, I. T.; Lee, G. H.; Chung, W. S. *J. Org. Chem.* **2007**, *72*, 2434−2442.
(28) Coskun, A.; Yilmaz, M. D.; Akkaya, E. U. *Org. Lett.* **2007**, *9*, 607−609.
(29) Ng, S. C.; Zhou, X. C.; Chen, Z. K.; Miao, P.; Chan, H. S. O.; Li, S. F. Y.; Fu, P. *Langmuir* **1998**, *14*, 1748−1752.
(30) Yuan, M. L. Y.; Li, J.; Li, C.; Liu, X.; Lv, J.; Xu, J.; Liu, H.; Wang, S.; Zhu, D. *Org. Lett.* **2007**, *9*, 2313−2316.
(31) Moon, S. Y.; Cha, N. R.; Kim, Y. H.; Chang, S. K. *J. Org. Chem.* **2004**, *69*, 181−183.
(32) Lee, C. H.; Lindsey, J. S. *Tetrahedron* **1994**, *50*, 11427−11440.
(33) Littler, B. J.; Miller, M. A.; Hung, C. H.; Wagner, R. W.; O'Shea, D. F.; Boyle, P. D.; Lindsey, J. S. *J. Org. Chem.* **1999**, *64*, 1391−1396.
(34) Kee, H. L.; Kirmaier, C.; Yu, L. H.; Thamyongkit, P.; Youngblood, W. J.; Calder, M. E.; Ramos, L.; Noll, B. C.; Bocian, D. F.; Scheidt, W. R.; Birge, R. R.; Lindsey, J. S.; Holten, D. *J. Phys. Chem. B* **2005**, *109*, 20433−20443.
(35) Angelici, R. J. *Organometallics* **2001**, *20*, 1259−1275.
(36) Choi, S. H.; Kim, K.; Lee, J.; Do, Y.; Churchill, D. G. *J. Chem. Crystallogr.* **2007**, *37*, 315−331.
(37) Maiti, N.; Lee, J.; Kwon, S. J.; Kwak, J.; Do, Y.; Churchill, D. G. *Polyhedron* **2006**, *25*, 1519−1530.
(38) Ko, S.; Park, S. H.; Gwon, H. J.; Lee, J.; Kim, M. J.; Kwak, Y.; Do, Y.; Churchill, D. G. *Bull. Korean Chem. Soc.* **2006**, *27*, 243−250.
(39) Goze, C.; Ulrich, G.; Mallon, L. J.; Allen, B. D.; Harriman, A.; Ziessel, R. **2006**, *128*, 10231−10239.
(40) Ulrich, G.; Goze, C.; Goeb, S.; Retailleau, P.; Ziessel, R. *New J. Chem.* **2006**, *30*, 982−986.
(41) Haugland, R. P.; Kang, H. C. (Molecular Probes, Inc., U.S.A.). U.S. Patent 5248782, 1993.
(42) Churchill, D. G. *J. Chem. Educ.* **2006**, *83*, 1798−1803.
(43) Maiti, N.; Lee, J.; Do, Y.; Shin, H. S.; Churchill, D. G. *J. Chem. Crystallogr.* **2005**, *35*, 949−955.

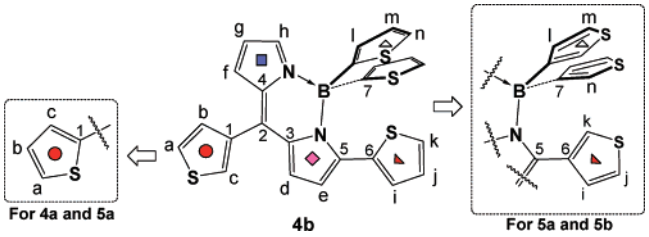

Figure 2. Atom designations and color/shape coding used herein in the assignment of NMR spectroscopic signals for derivatives **4a**−**5b**.

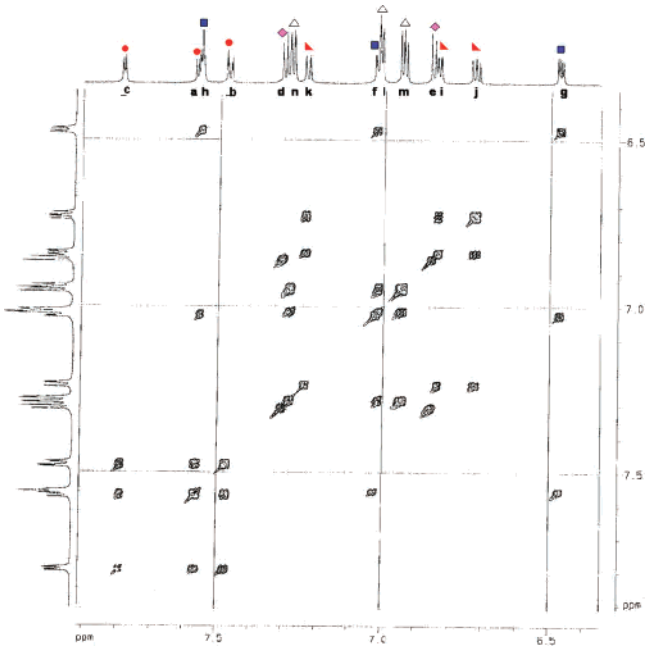

Figure 3. ^{1}H−^{1}H COSY contour plot containing all proton signals for **4b** in CH_2Cl_2 (400 MHz, RT). Color/shape coding comes from Figure 2.

chromatography (PTLC) (20 × 20 cm, 60 F silica gel) and (ii) TLC (cut from said PTLC plates) were obtained from Merck. The silica gel used in column chromatography was of diameter 0.04−0.063 mm. Melting points of **4a**−**5b** were taken in triplicate for each and respective average values are reported below.

Spectroscopy. All solvents used in NMR spectral analysis were of spectroscopic grade and purchased commercially. One-dimensional ^{1}H and ^{13}C NMR spectra (Figures 1-S−8-S) as well as COSY, NOESY, HMQC, and HMBC spectra (Figures 3−6; Figures 9-S−14-S) were measured on a Bruker Avance 400 MHz spectrometer with TMS used as an internal standard. ^{1}H and ^{13}C NMR spectral signals (in CD_2Cl_2) were further calibrated: δ 5.32 (^{1}H NMR) and δ 53.8 (^{13}C NMR). ^{11}B NMR spectra were measured by a Bruker 96 MHz spectrometer in which $F_3B{\cdot}OEt_2$ was used as an external standard. C, H, and N elemental analyses were measured using a Vario EL III elemental analyzer. UV−vis absorption and emission spectra were obtained using a Jasco V-530 UV−vis spectrometer (400 nm/min) and a Spectra CQ JOBIN YVON SPEX (Fluorolog, Horiba Group, 1 nm/s). Excitation wavelengths for the emission spectra were as follows: 563 (**4a**), 553 (**4b**), 539 (**5a**), and 531 nm (**5b**). High-resolution MALDI-TOF mass spectrometry was performed on an Applied Biosystem Voyager 4394 (ionization method, N_2 laser (337 nm, 3 ns pulse): analyzer 2.0 m linear mode; 3.0 m reflector mode). A Vilber Lourmat-4LC UV lamp (4W-365 nm, 50/60 Hz) was used to probe the fluorescence of reaction "spots" assayed by TLC.

X-ray Structure Determinations of 4b, 5a, and 5b. Crystals of **4b**, **5a**, and **5b** suitable for diffraction studies were grown from

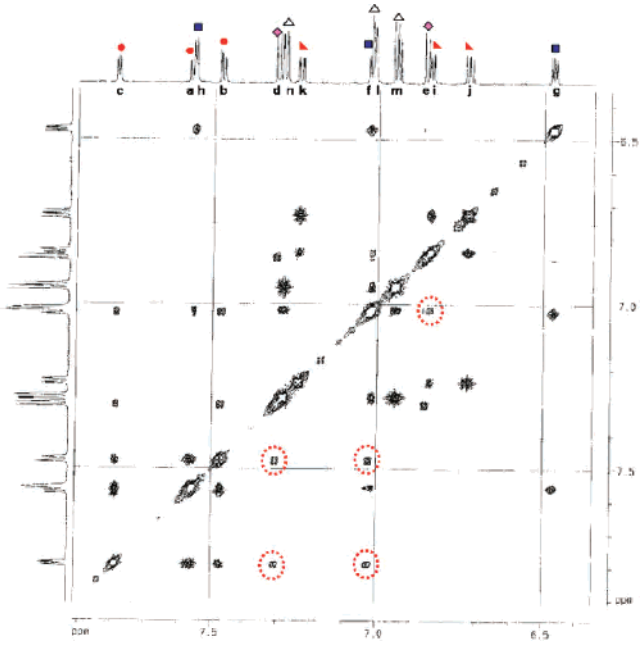

Figure 4. NOESY contour plot containing all proton signals for **4b** in CD_2Cl_2 (400 MHz, RT). Cross-peaks for through-space interactions between the pairs H_c−H_d, H_c−H_f, H_b−H_d, H_b−H_f, and H_i−H_l are encircled.

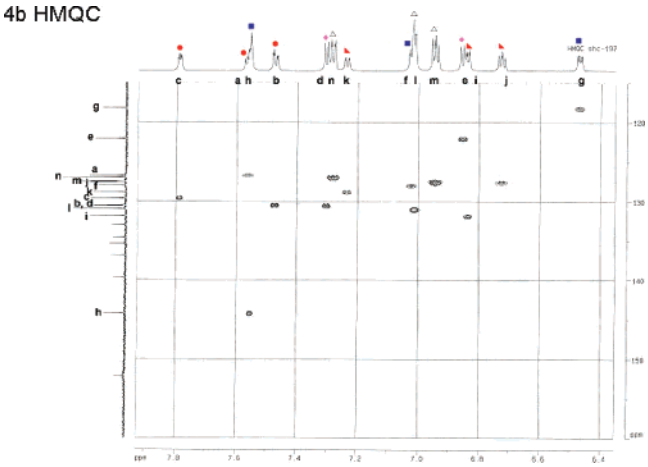

Figure 5. HMQC contour plot containing all proton and carbon signals used to assign tertiary carbon atoms for **4b** (CD_2Cl_2, 400 MHz, RT).

hexane and CH_2Cl_2 via slow evaporation at room temperature. Attempts at crystallizing **4a** likewise were undertaken but failed. Crystal sizes were 0.20 mm × 0.02 mm × 0.02 mm (**4b**), 0.2 mm × 0.2 mm × 0.35 mm (**5a**), and 0.25 mm × 0.25 mm × 0.25 mm (**5b**). Reflection data for **4b**, **5a**, and **5b** were collected on a Bruker P4 diffractometer equipped with a SMART CCD detector. Crystal data, data collection, and refinement parameters are summarized in Table 2 (also see Supporting Information). The structures were solved using direct methods and standard difference map techniques and refined by full-matrix least-squares procedures on F^2 with SHELXTL (Version 5.10)[44] (see Supporting Information). Some thienyl moieties in the prospective solutions for compounds **4b** and **5b** were disordered by a ca. 180° rotation about the respective $C_{dipyrrin}$−$C_{thienyl}$ or B−$C_{thienyl}$ vector as evidenced by distortions in the atomic thermal parameters upon least-squares refinement of the initial solution. Such crystallographic disorder was previously

(44) Sheldrick, G. M. *SHELXTL, An Integrated System for Solving, Refining and Displaying Crystal Structures from Diffraction Data*; University of Gottingen: Gottingen, Germany, 1981.

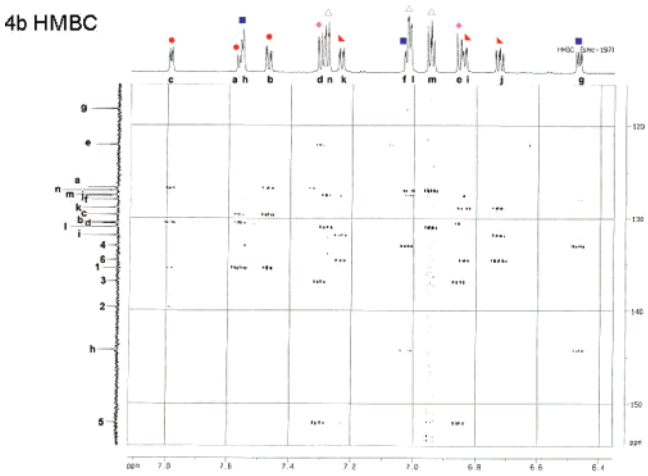

Figure 6. HMBC contour plot containing all proton and carbon signals used to assign remaining quaternary carbon atoms for **4b** (CD_2Cl_2, 400 MHz, RT).

Table 1. Spectral Properties in CH_3CN at RT

compound	$\lambda_{abs,max}$ (nm)	ϵ (M^{-1} cm^{-1})	$\lambda_{em,max}$ (nm)	Stokes' shift[a] (nm)	ϕ_F[b]
3a[c]	505	34 000	616	111	0.0079
3b[c]	498	51 000	518	20	0.078
4a	563	44 000	593	30	0.00058
4b	553	29 000	578	25	0.012
5a	539	33 000	575	36	0.00090
5b	531	41 000	562	31	0.0051

[a] Stokes' shifts were calculated from respective absorption and emission wavelengths. [b] Quantum yields were referenced using fluorescein[34] dissolved in 0.1 N NaOH as a reference ($\phi = 0.93$). [c] Spectra for compounds **3a** and **3b** have been remeasured.[36]

Table 2. X-ray Diffraction Study Parameters for **4b**, **5a**, and **5b**

	4b	**5a**	**5b**
chemical formula	$C_{25}H_{17}BN_2S_4$	$C_{25}H_{17}BN_2S_4$	$C_{25}H_{17}BN_2S_4$
fw	484.46	484.46	484.46
space group (No.)	$P2_1/n$ (14)	$P\bar{1}$ (2)	$\bar{P}1$ (2)
a (esd), Å	8.388(2)	10.0954(5)	10.1117(6)
b (esd), Å	9.059(2)	10.0984(5)	10.1902(6)
c (esd), Å	29.546(8)	12.9732(6)	13.0217(7)
α (esd), deg	90	76.6430(10)	75.6350(10)
β (esd), deg	93.666(4)	72.4810(10)	71.7000(10)
γ (esd), deg	90	64.6380(10)	64.2070(10)
V (esd), Å^3	2240.5(10)	1131.66(9)	1137.19(11)
Z	4	2	2
μ (mm^{-1})	0.441	0.437	0.435
R1[a]	0.0778	0.1287	0.0765
wR2[b]	0.1737	0.4276	0.2370
ρ_{calcd} (mg/m^3)	1.436	1.422	1.415
T (K)	243(2)	243(2)	243(2)

[a] $R1 = (\sum||F_o| - |F_c||)/\sum|F_o|$. [b] $wR2 = [(\sum(F_o^2 - F_c^2)^2)/\sum w(F_o^2)^2]^{1/2}$.

encountered in related dipyrromethane[43] and BF_2−dipyrrin derivatives.[36] Modeling of this disorder involved creating atomic coordinates for a second thienyl group; both parts were least-squares refined. Requisite cif files of the crystallographic determinations of **4b**−**5b** have been deposited with the Cambridge Crystallographic Data center (CCDC): CCDC 641774 (**4b**), CCDC 641776 (**5a**), and CCDC 641775 (**5b**).

Synthesis of 4a. Compound **3a**, which has been previously reported,[36] was prepared again, and a portion of it (1.35 g, 4.75 mmol) was dissolved in anhydrous THF (50 mL) and stirred at −78 °C for 10 min. Into this solution a sample of 2-thienyllithium (30 mL, 1.0 M in THF) was added slowly. The reaction mixture was stirred at −78 °C for 10 min before being warmed to RT. After complete consumption of **3a**, the reaction was quenched with water (ca. 20 mL). The reaction mixture was then extracted with CH_2Cl_2 and dried over magnesium sulfate (excess). After filtration away from the drying agent and removal of the solvent the contents of the filtrate were then purified by way of silica gel column chromatography (×3) using a mixture of hexane and CH_2Cl_2 as the eluent. A deep pink fraction (red fluorescent) ($R_f = 0.7-0.8$, similar for all **4a**−**5b**) was isolated but was still deemed to be impure via TLC assay. Further purification was undertaken by PTLC (preparative TLC) (×3). See Supporting Information. A pure sample of compound **4a** was finally isolated via recrystallization (0.70 g, 31%). Melting point: 163 °C.[45] ^{1}H NMR (CD_2Cl_2, δ 5.32): 7.72 (dd, $^3J_{H-H} = 5.0$, $J_{H-H} = 0.8$ Hz, 1H$_b$), 7.62 (d, $^3J_{H-H} = 4.0$ Hz, 1H$_c$), 7.58 (s, 1H$_h$), 7.48 (d, $^3J_{H-H} = 4.6$ Hz, 1H$_d$), 7.30 (m, 2H$_n$), 7.28 (s, 1H$_a$), 7.25 (dd, $^3J_{H-H} = 0.6$, $^4J_{H-H}$ 0.6 Hz, 1H$_k$), 7.21 (dd, $^3J_{H-H} = 4.5$, $^4J_{H-H} = 0.9$ Hz, 1H$_f$), 7.04 (d, $^3J_{H-H} = 3.3$ Hz, 2H$_l$), 6.96 (m, 2H$_m$), 6.88 (d, $^3J_{H-H} = 4.6$ Hz, 1H$_e$), 6.87 (s, 1H$_i$), 6.74 (dd, $^3J_{H-H} = 4.8$, $^3J_{H-H} = 4.0$ Hz, 1H$_j$), 6.49 (dd, $^3J_{H-H} = 4.0$, $J_{H-H} = 1.9$ Hz, 1H$_g$). ^{13}C NMR (CD_2Cl_2, δ 53.8): 152.4 (t, $^1J_{C-H} = 8.8$ Hz, 1C$_5$), 144.5 (dt, $^1J_{C-H} = 185.0$, $^3J_{C-H} = 9.0$ Hz, 1C$_h$), 137.5 (s, 1C$_2$), 136.8 (t, $^2J_{C-H} = 9.0$ Hz, 1C$_3$), 135.4 (p, $^2J_{C-H} = 5.6$ Hz, 1C$_1$), 134.5 (m, $J_{C-H} = 5.6$ Hz, 1C$_6$), 132.9 (m, 1C$_4$), 132.8 (ddd, $^1J_{C-H} = 169.6$ Hz, $^2J_{C-H} = 9.3$ Hz, $^3J_{C-H} = 6.1$ Hz, 1C$_c$), 132.0 (ddd, $^1J_{C-H} = 163.4$ Hz, $^3J_{C-H} = 9.2$ Hz, $^3J_{C-H} = 6.0$ Hz, 1C$_i$), 131.0 (dm, $^1J_{C-H} = \sim160$ Hz, 1C$_l$), (dm, $^1J_{C-H} = \sim160$ Hz, 1C$_d$), 130.7 (ddd, $^1J_{C-H} = \sim200$, $^2J_{C-H} = 9.2$, $^3J_{C-H} = 6.1$ Hz, 1C$_b$), 129.0 (dm, $^1J_{C-H} = 211.3$ Hz, 1C$_k$), 128.5 (m, 1C$_f$), 128.2 (dt, $^1J_{C-H} = 171.0$, $^2J_{C-H} = 10.1$ Hz, 1C$_a$), 127.6 (dm, $^1J_{C-H} = 161.0$ Hz, 1C$_j$), 127.5 (dm, $^1J_{C-H} = 161.0$ Hz, 2C$_m$), 127.1 (dm, $^1J_{C-H} = 201.2$ Hz, 2C$_n$), 122.3 (dd, $^1J_{C-H} = 175.2$, $^2J_{C-H} = 3.6$ Hz, 1C$_e$), 118.4 (ddd, $^1J_{C-H} = 174.8$, $^3J_{C-H} = 8.9$, $^3J_{C-H} = 3.5$ Hz, 1C$_g$). ^{11}B NMR ($F_3B{\cdot}OEt_2$, δ 0.00): −3.59 (s). MALDI-TOF *m*/*z* (M^+): 484.04 (calcd); 483.99 (obs). Anal. Calcd for $C_{25}H_{17}BN_2S_4$: C, 61.98; H, 3.54; N, 5.78. Found: C, 63.44; H, 3.81; N, 6.00.

Synthesis of 4b. The preparation of **4b** was performed via the same procedure as for **4a** with **3b** (0.18 g, 0.65 mmol) being used in place of **3a** and 2-thienyllithium (6.5 mL, 1.0 M in THF). After reaction, by TLC inspection, a strong red fluorescent fraction ($R_f = 0.8$, CH_2Cl_2) was present and through silica gel column chromatography (×3) and PTLC (×3) (see Supporting Information), a pure sample of **4b** was obtained. Crystalline material of **4b** was obtained by recrystallization from a solution of hexane and CH_2Cl_2 (30:1 ratio by volume) (0.12 g, yield 35%). Melting point: 166 °C. ^{1}H NMR (CD_2Cl_2, δ 5.32): 7.79 (dd, $^4J_{H-H} = 3.0$, $^4J_{H-H} = 1.2$ Hz, 1H$_c$), 7.57 (d, $J = 3.0$ Hz, 1H$_a$), 7.56 (m, 1H$_h$), 7.48 (dd, $^3J_{H-H} = 5.0$, $^4J_{H-H} = 1.2$ Hz, 1H$_b$), 7.30 (d, $^3J_{H-H} = 4.5$ Hz, 1H$_d$), 7.29 (dd, $^3J_{H-H} = 4.7$, $^4J_{H-H} = 0.8$ Hz, 2H$_n$), 7.24 (dd, $^3J_{H-H} = 5.0$, $^4J_{H-H} = 1.1$ Hz, 1H$_k$), 7.03 (d, $^3J_{H-H} =$ obs, $^4J_{H-H} = 1.3$ Hz, 1H$_f$), 7.02 (dd, $^3J_{H-H} = 3.4$, $^4J_{H-H} = 1.0$ Hz, 2H$_l$), 6.95 (m, 2H$_m$), 6.85 (d, $^3J_{H-H} = 4.5$ Hz, 1H$_e$), 6.84 (dd, $^3J_{H-H} = 3.7$, $^4J_{H-H} = 1.1$ Hz, 1H$_i$), 6.73 (dd, $^3J_{H-H} = 5.1$, $^4J_{H-H} = 3.7$ Hz, 1H$_j$), 6.47 (dd, $^3J = 4.2$, 1.9 Hz, 1H$_g$). ^{13}C NMR (CD_2Cl_2, δ 53.8): 152.1 (m, 1C$_5$), 144.3 (dt, $^1J_{C-H} = 184.9$, $^3J_{C-H} = 9.1$ Hz, 1C$_h$), 139.7 (s, 1C$_2$), 136.9 (t, $^2J_{C-H} = 9.0$ Hz, 1C$_3$), 135.4 (m, 1C$_1$), 134.6 (m, 1C$_6$), 133.0 (q, $^2J_{C-H} = 8.8$ Hz, 1C$_4$), 131.9 (ddd, $^1J_{C-H} = 170.7$, $^2J_{C-H} = 9.2$, 1C$_i$), 130.9 (ddd, $^1J_{C-H} = 163.3$, $^2J_{C-H} = 9.8$, 1C$_l$), 130.5 (dm, $^1J_{C-H} = 171.9$, 1C$_b$), 130.4 (dm, $^1J_{C-H} = 165.4$ Hz, 1C$_d$), 129.6 (dm, $^1J_{C-H} = 171.0$ Hz, 1C$_c$), 128.9 (dm, $^1J_{C-H} = 186.2$ Hz, 1C$_k$), 127.9 (dm, $^1J_{C-H} = 161.0$, 1C$_f$), 127.6 (dm, $^1J_{C-H} = 170.8$, 1C$_j$), 127.5 (dm, $^1J_{C-H} = 168.7$, 2C$_m$), 127.0 (ddd, $^1J_{C-H} =$

(45) The melting point values obtained for **3a** and **3b** are 111 and 152 °C, respectively.

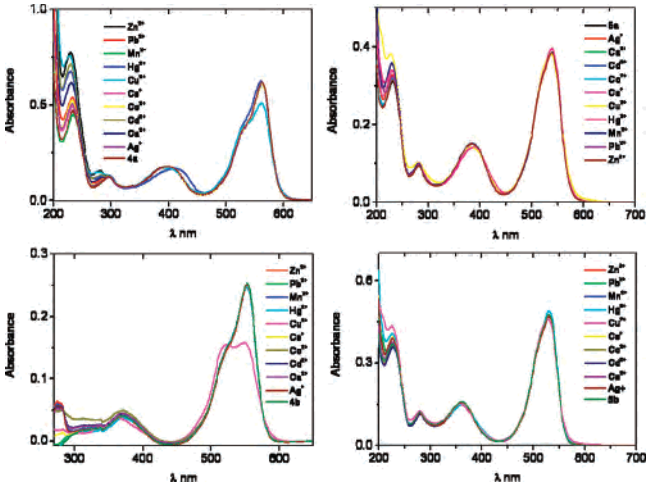

Figure 7. Absorption spectra in CH_3CN for ligand−metal ion (1:1) mixtures in CH_3CN. **4a**−**5b** are at 1.0×10^{-5} M, and M^{2+} or M^{+} are at 1×10^{-3} M.

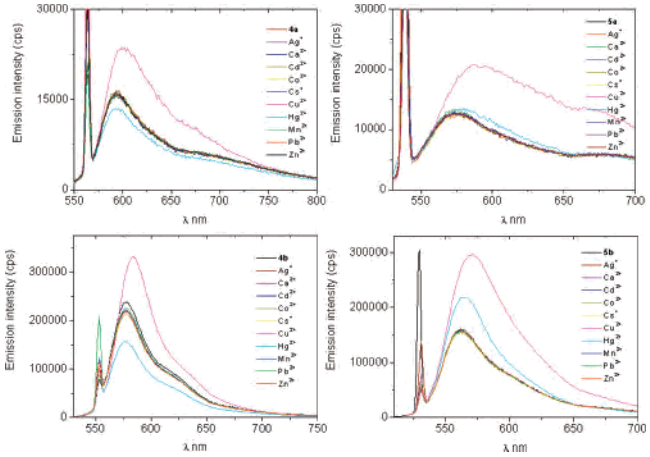

Figure 8. Emission spectra of 1:1 mixtures of ligand:metal ion mixtures in CH_3CN. Ligands **4a**−**5b** are at 1.0×10^{-5} M, and M^{2+} or M^{+} are at 1×10^{-3} M. Excitation wavelengths were as follows: 563 (**4a**), 553 (**4b**), 539 (**5a**), and 531 nm (**5b**).

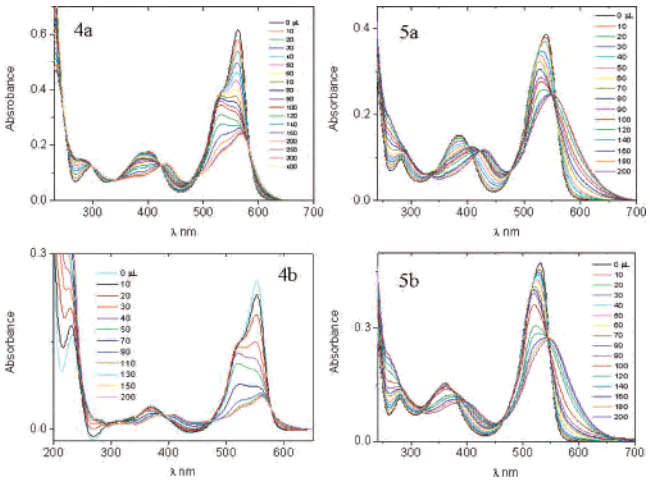

Figure 9. Absorption spectra of **4a** (top left), **4b** (bottom left), **5a** (top right), and **5b** (bottom right) upon titration with Cu^{2+} in CH_3CN. Ligands **4a**−**5b** are at 1.0×10^{-5} M, and the added Cu^{2+} solution concentration was 1.0×10^{-3} M.

184.2, $^2J_{C-H} = 10$, $^3J_{C-H} = 7.8$ Hz, $2C_n$), 126.7 (dt, $^1J_{C-H} = 186.8$, $^3J_{C-H} = 6.9$ Hz, $1C_a$), 122.1 (dd, $^1J_{C-H} = 175.1$, $^3J_{C-H} = 3.7$ Hz, $1C_e$), 118.3 (ddd, $^1J_{C-H} = 174.6$, $^3J_{C-H} = 8.9$, $^3J_{C-H} = 3.7$ Hz, $1C_g$). ^{11}B NMR ($F_3B{\cdot}OEt_2$, δ 0.00): −3.61 (s). MALDI-TOF *m*/*z* (M^+): 484.04 (calcd), 484.36 (obs). Anal. Calcd for $C_{25}H_{17}BN_2S_4$: C, 61.98; H, 3.54; N, 5.78. Found: C, 62.63; H, 4.21; N, 5.66.

Synthesis of 5a. First, an adequate amount of 3-thienyllithium was prepared according to a literature method:[46] 3-bromothiophene (1.6 mL, 0.017 mol) was diluted in anhydrous ether (50 mL) and stirred at −78 °C under Ar. Into this solution, *n*-BuLi (5.44 mL, 2.5 M in hexane) was added dropwise. The reaction mixture was stirred for 10 min. Separately, **3a** (0.46 g, 0.0017 mol) was dissolved in anhydrous THF (12 mL) at room temperature. This solution was then transferred to the 3-thienyllithium solution slowly. The reaction mixture was stirred at −78 °C under Ar. The starting compound **3a** was completely consumed after 10 min, and the reaction was quenched with water, extracted with CH_2Cl_2, and dried over magnesium sulfate. After filtration away from the drying agent and removal of the solvent, the contents of the filtrate were then purified by way of silica gel chromatography (×3); the crude material was additionally purified via PTLC (×3) (see Supporting Information) with a hexane and CH_2Cl_2 eluent (2:1 by volume) (0.088 g, yield 11%). Melting point: 184 °C. ^{1}H NMR (CD_2Cl_2, δ 5.32): 7.71 (dd, $^3J_{H-H} = 5.1$, $^4J_{H-H} = 1.2$ Hz, $1H_b$), 7.61 (dd, $^3J_{H-H} = 3.7$, $^4J_{H-H} = 1.2$ Hz, $1H_c$), 7.46 (d, $^3J_{H-H} = 4.4$ Hz, $1H_d$), 7.41 (m, $1H_h$), 7.28 (m, $1H_a$), 7.19 (dd, $^3J_{H-H} = 4.3$, $^4J_{H-H} = 1.3$ Hz, $1H_f$), 7.15 (dd, $^3J_{H-H} = 4.8$, $^3J_{H-H} = 2.7$ Hz, $2H_m$), 7.01 (m, $1H_j$), 6.97 (m, $1H_k$), 6.94 (dd, $^4J_{H-H} = 2.7$, $^4J_{H-H} = 1.1$ Hz, $2H_n$), 6.89 (dd, $^3J_{H-H} = 4.8$, $^4J_{H-H} = 1.1$ Hz, $2H_l$), 6.81 (dd, $^3J_{H-H} = 5.0$, $^4J_{H-H} = 1.3$ Hz, $2H_i$), 6.74 (d, $^3J_{H-H} = 4.4$ Hz, $1H_e$), 6.46 (dd, $^3J_{H-H} = 4.2$, $^4J_{H-H} = 1.8$ Hz, $1H_g$). ^{13}C NMR (CD_2Cl_2, δ 53.8): 154.6 (t, $^1J_{C-H} = 8.2$ Hz, $1C_5$), 143.6 (dt, $^1J_{C-H} = 184.6$, $^3J_{C-H} = 9.0$ Hz, $1C_h$), 138.0 (s, $1C_2$), 136.4 (t, $^1J_{C-H} = 9.0$ Hz, $1C_3$), 135.6 (m, $1C_1$), 133.4 (m, $1C_6$), 133.1 (m, $1C_4$), 132.8 (ddd, $^1J_{C-H} = 170.0$, $^2J_{C-H} = 9.3$, $^3J_{C-H} = 5.8$ Hz, $1C_c$), 132.2 (dm, $^1J_{C-H} = 152.1$ Hz, $1C_l$), 130.7 (dm, $^1J_{C-H} = 169.6$ Hz, $1C_d$), 130.5 (ddd, $^1J_{C-H} = 184.9$, $^2J_{C-H} = 10.8$, $^2J_{C-H} = 7.1$ Hz, $1C_b$), 129.2 (ddd, $^1J_{C-H} = 171.1$, $^3J_{C-H} = 10$, $^3J_{C-H} = 3.6$ Hz, $1C_i$), 128.1 (dm, $^1J_{C-H} = 180.9$ Hz, $1C_a$), 128.0 (dm, $^1J_{C-H} = \sim 170$ Hz, $1C_f$), 128.0 (dm, $^1J_{C-H} = \sim 170$ Hz, $1C_k$), 127.7 (ddd, $^1J_{C-H} = 160.8$, $^3J_{C-H} = 8.5$, $^3J_{C-H} = 4.2$ Hz, $1C_n$), 124.6 (ddd, $^1J_{C-H} = 183.2$, $J_{C-H} = 4.7$ Hz, $1C_m$), 124.1 (ddd, $^1J_{C-H} = 187.6$, $^3J_{C-H} = 6.2$, $^3J_{C-H} = 4.7$ Hz, $1C_j$), 121.6 (dd, $^1J_{C-H} = 174.4$, $^3J_{C-H} = 3.5$ Hz, $1C_e$), 117.8 (ddd, $^1J_{C-H} = 174.5$, $^3J_{C-H} = 9.1$, $^3J_{C-H} = 3.6$ Hz, $1C_g$). ^{11}B NMR ($F_3B{\cdot}OEt_2$, δ 0.00): −3.59 (s). MALDI-TOF *m*/*z* (M^+): 484.04 (calcd), 484.68 (obs). Anal. Calcd for $C_{25}H_{17}BN_2S_4$: C, 61.98; H, 3.54; N, 5.78. Found: C, 63.68; H, 3.82; N, 6.03.

Synthesis of 5b. The preparation of **5b** involved the same procedure as that for **5a** except using **3b** (1 g, 3.65 mmol) in place of **3a**. 3-Bromothiophene (3.5 mL, 36.5 mol) was diluted in anhydrous diethyl ether (50 mL) and stirred at −78 °C under Ar. Into this solution, *n*-BuLi (12 mL, 2.5 M in hexane) was added dropwise, and the reaction mixture was stirred for ca. 10 min. After this time **3b**, dissolved in anhydrous THF (20 mL), was transferred to the 3-thienyllithium solution slowly. The reaction mixture was stirred at −78 °C under Ar for 10 min before being allowed to warm to room temperature. After verifying an adequate consumption of **3b**, the reaction mixture was quenched with water, extracted with CH_2Cl_2, and dried over magnesium sulfate. After filtration away from the drying agent and removal of the solvent, the contents of the filtrate were then purified by way of silica gel column chromatography (×3) using a hexane:CH_2Cl_2 mixture (2:1−1:2

(46) Karlsson, L.; Bergmark, T.; Jadrny, R.; Siegbahn, K.; Gronowitz, S.; Maltesson, A. *Chem. Scr.* **1974**, *6*, 214−221.

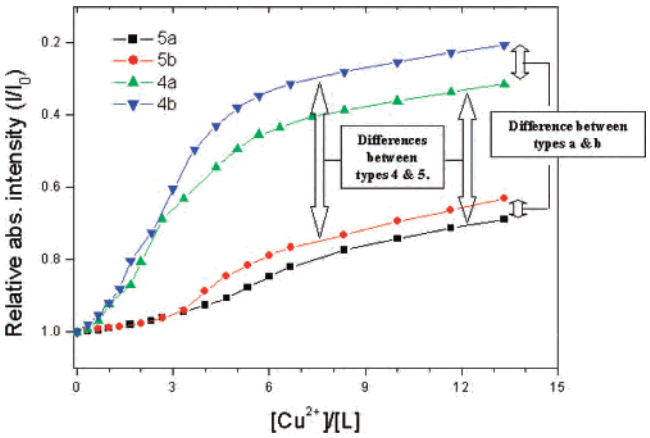

Figure 10. Absorbance changes upon Cu^{2+} titration at respective values of $\lambda_{abs\ max}$ (Figure 9) as a function of $[Cu^{2+}]/[ligand]$ (ligand: **4a**, **4b**, **5a**, and **5b**).

gradient by volume). The crude mixture was purified several times by PTLC (eluent, hexane:CH_2Cl_2, 5:1) (see Supporting Information), and finally, red crystals exhibiting green fluorescence were obtained by recrystallization using a hexane−CH_2Cl_2 mixture (30:1 ratio by volume) (0.15 g, yield 8.5%). Melting point: 178 °C. ^{1}H NMR (CD_2Cl_2, δ 5.32): 7.78 (dd, $^4J_{H-H}$ = 3.0, $^4J_{H-H}$ = 1.2 Hz, 1H$_c$), 7.55 (m, 1H$_a$), 7.47 (dd, $^3J_{H-H}$ = 5.0, $^4J_{H-H}$ = 1.2 Hz, 1H$_b$), 7.43 (m, 1H$_h$), 7.30 (d, $^3J_{H-H}$ = 4.5 Hz, 1H$_d$), 7.17 (dd, $^3J_{H-H}$ = 4.7, $^4J_{H-H}$ = 2.7 Hz, 2H$_m$), 7.03 (d, $^3J_{H-H}$ = obs, $^4J_{H-H}$ = 1.2 Hz, 1H$_f$), 7.02 (m, 1H$_j$), 6.98 (m, 1H$_k$), 6.96 (dd, J = 2.7, 1.1 Hz, 2H$_n$), 6.91 (dd, J = 4.8, 1.1 Hz, 2H$_l$), 6.83 (dd, $^3J_{H-H}$ = 5.0, $^4J_{H-H}$ = 1.4 Hz, 1H$_i$), 6.73 (d, $^3J_{H-H}$ = 4.5 Hz, 1H$_e$), 6.46 (dd, $^3J_{H-H}$ = 4.2, J_{H-H} = 1.8 Hz, 1H$_g$). ^{13}C NMR (CD_2Cl_2, δ 53.8): 154.3 (m, 1C$_5$), 152.4 (br, 1C$_7$), 143.4 (dt, $^1J_{C-H}$ = 184.4, $^3J_{C-H}$ = 9.0, 1C$_h$), 140.1 (s, 1C$_2$), 136.4 (t, $^1J_{C-H}$ = 9.0 Hz, 1C$_3$), 135.6 (m, 1C$_1$), 133.5 (m, 1C$_6$), 133.2 (d, $^1J_{C-H}$ = 8.7 Hz, 1C$_4$), 132.2 (ddd, $^1J_{C-H}$ = 164.9, $^2J_{C-H}$ = 10.5, $^3J_{C-H}$ = 4.9 Hz, C$_l$), 130.5 (ddd, $^1J_{C-H}$ = 173.0, $^2J_{C-H}$ = 8.5, $^3J_{C-H}$ = 4.7 Hz, 1C$_b$), 130.2 (dd, $^1J_{C-H}$ = 175.1, $^3J_{C-H}$ = 4.2 Hz, 1C$_d$), 129.4 (dm, $^1J_{C-H}$ = 185.8 Hz, 1C$_c$), 129.2 (ddd, $^1J_{C-H}$ = 170.5, $^2J_{C-H}$ = 8.5, $^3J_{C-H}$ = 4.1 Hz, 1C$_i$), 128.0 (ddd, $^1J_{C-H}$ = 128.0, $^3J_{C-H}$ = 8.5, $^3J_{C-H}$ = 4.4 Hz, 1C$_k$), 127.6 (dm, $^1J_{C-H}$ = 152.4 Hz, C$_n$), 127.5 (dm, $^1J_{C-H}$ = 195.4 Hz, 1C$_f$), 126.6 (dm, $^1J_{C-H}$ = 188.8 Hz, 1C$_a$), 124.6 (ddd, $^1J_{C-H}$ = 189.6, $^2J_{C-H}$ = 9.0, $^3J_{C-H}$ = 4.7 Hz, 2C$_m$), 124.1 (dt, $^1J_{C-H}$ = 187.6 Hz, $^3J_{C-H}$ = 6.3, 1C$_j$), 121.4 (dd, $^1J_{C-H}$ = 171.1, $^2J_{C-H}$ = 3.5 Hz, 1C$_e$), 117.7 (ddd, $^1J_{C-H}$ = 174.3, $^3J_{C-H}$ = 9.0, $^3J_{C-H}$ = 3.7 Hz, 1C$_g$). ^{11}B NMR ($F_3B{\cdot}OEt_2$, δ 0.00): −3.35 (s). MALDI-TOF m/z (M^+): 484.04 (calcd), 484.41 (obs). Anal. Calcd for $C_{25}H_{17}BN_2S_4$: C, 61.98; H, 3.54; N, 5.78. Found: C, 62.56; H, 3.82; N, 5.88.

^{1}H−^{1}H and ^{1}H−^{13}C NMR Spectroscopic Experiments. For NMR spectroscopic measurements using CD_2Cl_2, the ligand samples were tightly sealed in an NMR tube fitted with a J. Young valve (Wilmad) to prevent solvent evaporation during the lengthy (2−16 h) RT NMR spectroscopic scan acquisitions.

Sample Preparation of UV−Vis Absorption and Emission Measurements. For UV−vis absorption and emission measurements, a sample of pure ligand (**4a**−**5b**) was dissolved in CH_3CN to give a solution of concentration 1.0×10^{-5} M. Separately, metal perchlorate salts[42] were dissolved in CH_3CN to give solutions with a concentration of 1.0×10^{-3} M. A clean quartz cuvette (5 mL, two- or four-face) was used while obtaining absorption and emission spectra. Photographs (e.g., Figure 12) were acquired by a Cybershot DSC-W70 digtal camera (Sony Corp).

Titrations. A 3.0 mL amount of ligand (**4a**−**5b**) solution was placed in the cuvette, and the metal-ion solution was added by

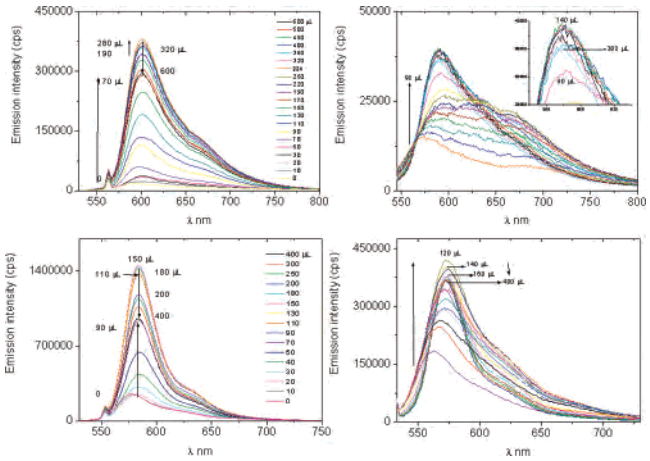

Figure 11. Emission spectra of **4a** (top left), **4b** (bottom left), **5a** (top right), and **5b** (bottom right) upon titration with Cu^{2+} in MeCN. Ligands **4a**−**5b** are at a concentration of 1.0×10^{-5} M, and Cu^{2+} is added at a concentration of 1.0×10^{-3} M. Excitation wavelengths were as follows: 563 (**4a**), 553 (**4b**), 539 (**5a**), and 531 nm (**5b**).

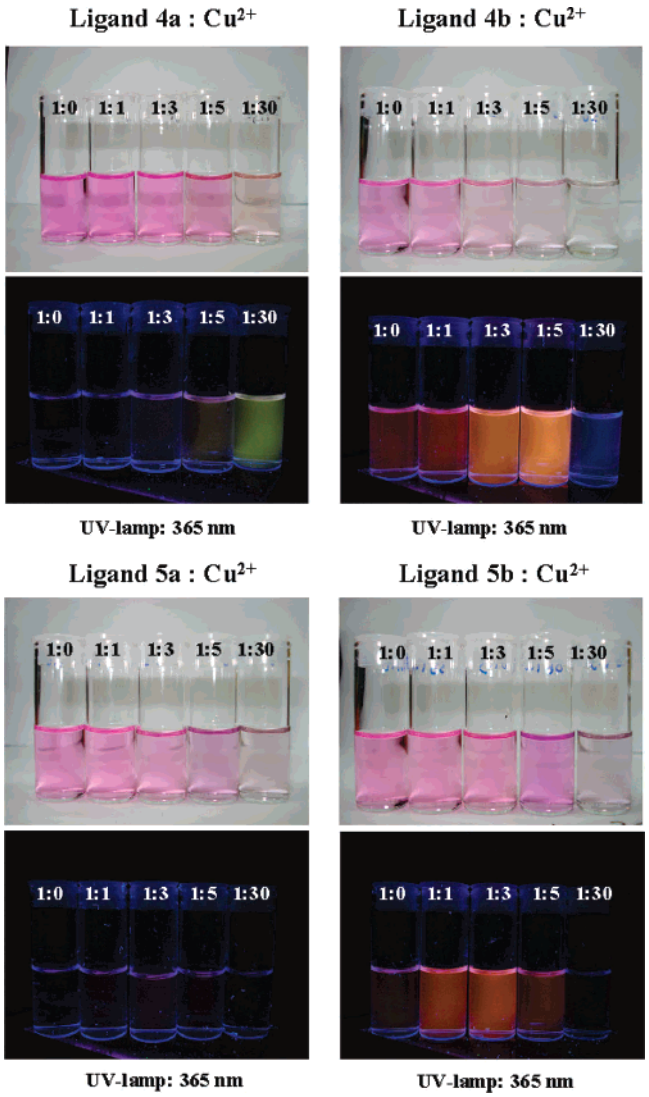

Figure 12. Photographs of 4 mL vials filled with various 1:n concentrations of Cu^{2+} and ligand under white light (top in each pair) and UV light (365 nm) (bottom in each pair).

micropipette. The mixture solution was lightly shaken and kept for 1 min before spectra were recorded.

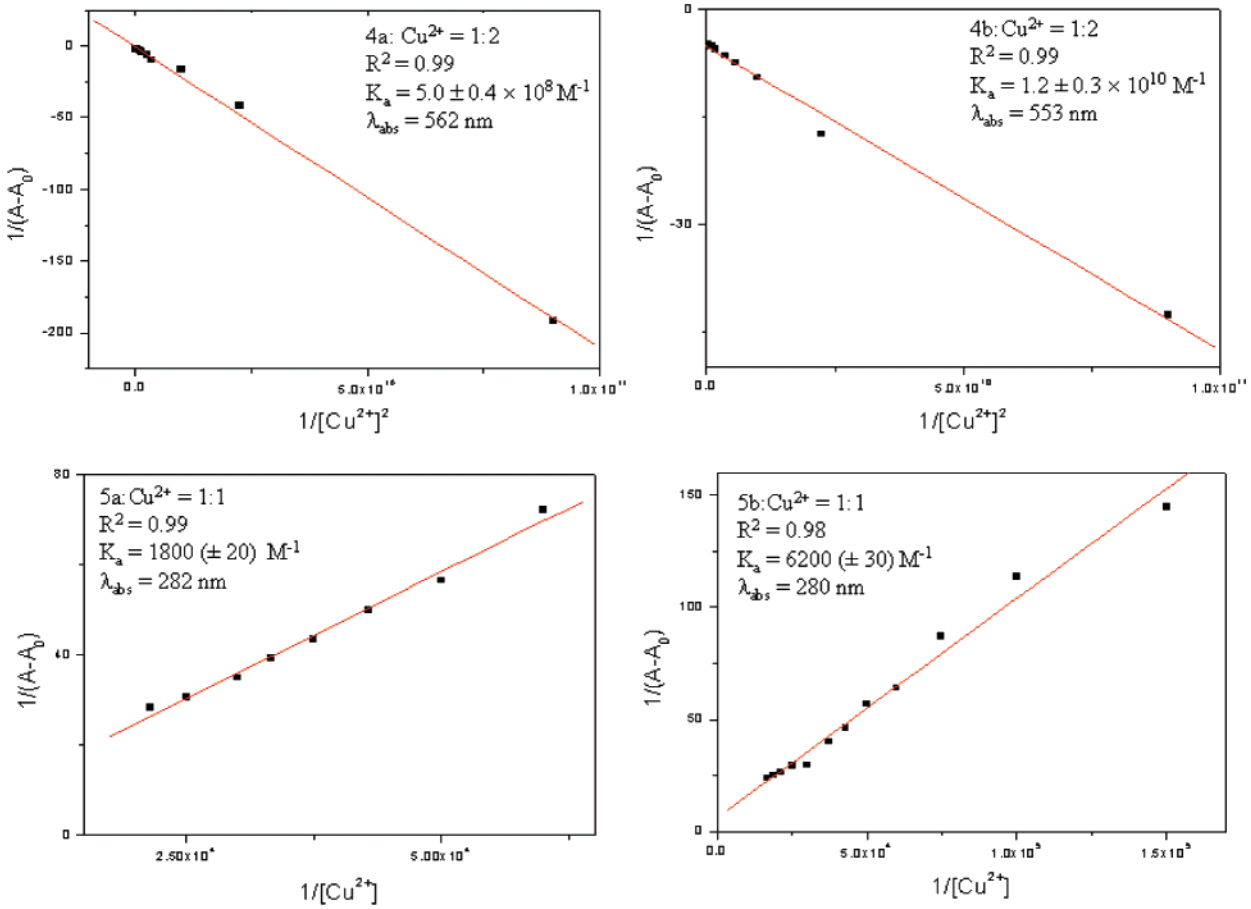

Figure 13. Modeling of ligand−Cu^{2+} binding constants using the Benesi−Hildebrand equation.

Competition Experiment Details. Ligand **4a** was dissolved in CH_3CN to achieve a concentration of 1×10^{-5} M. A 3 mL portion of this ligand solution was treated (injected) with 30 μL of M^{n+} solution (1×10^{-3} M, CH_3CN). The emission of the mixed solution was recorded at a given excitation wavelength (562 nm for **4a**, 553 nm for **4b**, 539 nm for **5a**, and 531 nm for **5b**). After this step, 30 μL of Cu^{2+} solution (1×10^{-3} M, CH_3CN) was added, and after mixing with the above ligand−M^{n+} solution the emission spectrum was recorded after ca. 1 min. The difference of emission intensity before and after addition of Cu^{2+} was obtained, and this data is displayed as bar graphs (Figure 14). This process was analogous for ligands **4b**, **5a**, and **5b**. ***Caution!*** *Perchlorate salts are a known explosion hazard.*[42]

Computational Details. The Gaussian 03 program was used for all calculational work.[47] All calculations were performed in the gas phase. Hardware used involved an in-house Intel Pentium IV 3.0 system(s). MO pictures were obtained by GaussView 3.0. The following protocol was used for all calculations: (a) input geometries were derived from the crystallographic structures provided herein except in the case of **4a**, which was derived by a careful modification of the geometry of **4b** and invoking chemical intuition; (b) density functional theory (DFT) geometry optimizations and single-point calculations were performed using the B3LYP/6-31++(G) basis set; after the geometry optimizations (c) vibrational frequencies were calculated for **4a**−**5b** and found to be zero in all cases.

3. Results and Discussion

Synthesis. The synthesis of complexes **4a**−**5b** illustrated in Scheme 1 involved four convenient steps from commercially available and inexpensive starting materials. Herein, three main literature transformations as reported in related systems were relied on for the first three steps here (Scheme 1, *i*−*iii*), namely, preparation of 5-substituted dipyrromethanes by Lindsey and co-workers,[32,33] oxidation of dipyromethanes to dipyrrins (dipyrromethenes) by Dolphin and co-workers,[48] and finally the early report regarding preparation of BF_2−dipyrrin by Treibs and Kreuzer.[49]

Specifically, in obtaining **4a**−**5b** condensation of pyrrole and the respective thienyl carboxylate gave the dipyrromethane as previously reported.[43] Next, oxidation of the dipyrrin gave pure BF_2−dipyrrin in sufficient amounts.[36] Finally, treatment of **3a** and **3b** with thienyllithium was performed with the expectation of obtaining bis-substituted boron analogues, but we actually generated significant amounts of the deep red, asymmetric multithienyl-substituted

(47) Frisch, M. J.; Trucks, G. W.; Schlegel, H. B.; Gill, P. M. W.; Johnson, B. G.; Robb, M. A.; Cheeseman, J. R.; Keith, T.; Petersson, G. A.; Montgomery, J. A.; Raghavachari, K.; Al-Laham, M. A.; Zakrzewski, V. G.; Ortiz, J. V.; Foresman, J. B.; Cioslowski, J.; Stefanov, B. B.; Nanayakkara, A.; Challacombe, M.; Peng, C. Y.; Ayala, P. Y.; Chen, W.; Wong, M. W.; Andres, J. L.; Replogle, E. S.; Gomperts, R.; Martin, R. L.; Fox, D. J.; Binkley, J. S.; Defrees, D. J.; Baker, J.; Stewart, J. P.; Head-Gordon, M.; Gonzalez, C.; Pople, J. A. *Gaussian 03*, Revision C.01; Gaussian, Inc.: Pittsburgh, PA, 2004.

(48) Bruckner, C.; Karunaratne, V.; Rettig, S. J.; Dolphin, D. *Can. J. Chem.* **1996**, *74*, 2182−2193.

(49) Treibs, A.; Kreuzer, F. H. *Ann. Chem.* **1968**, *718*, 208.

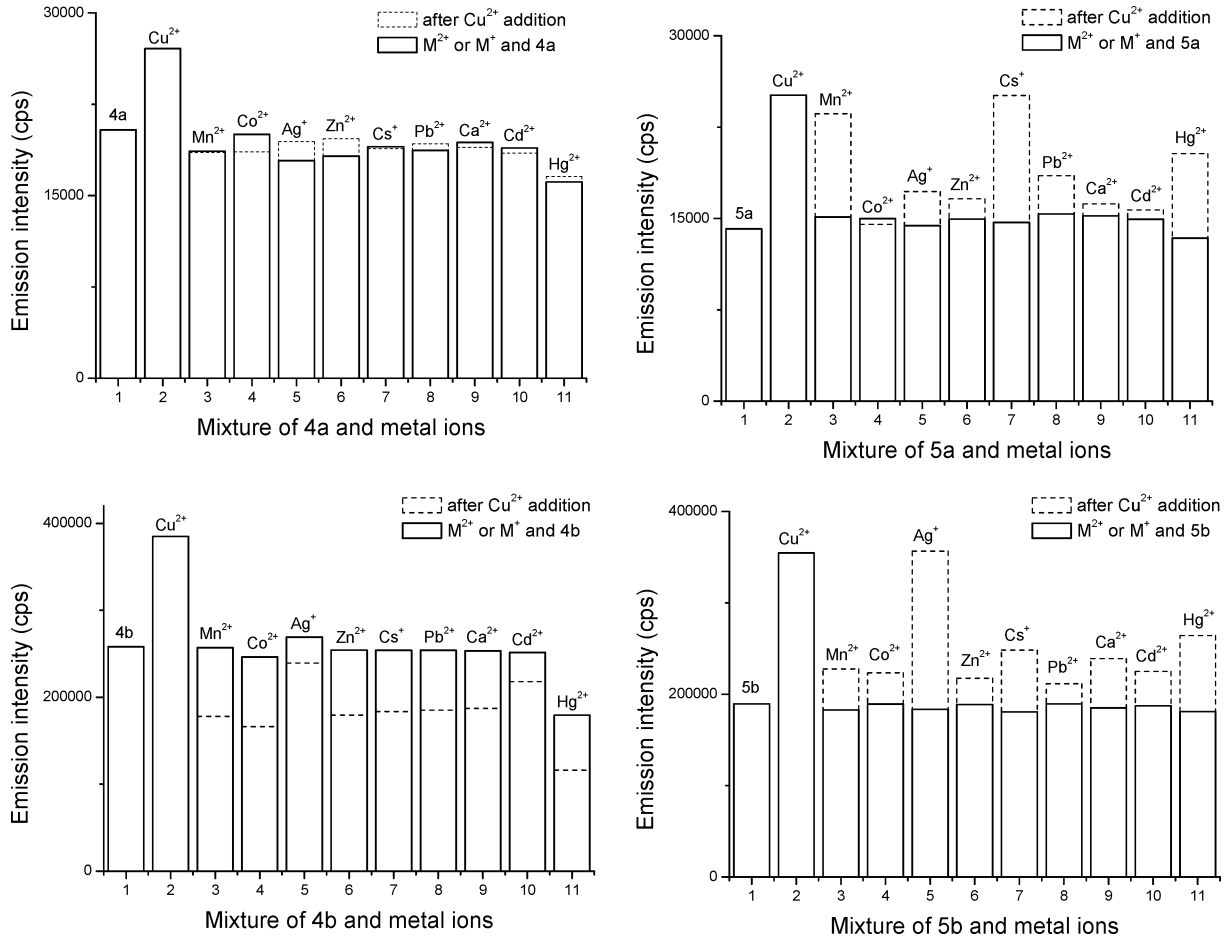

Figure 14. Emission intensity changes of $L-M^{n+}$ systems upon addition of Cu^{2+} in CH_3CN at 562 nm. $L:M^{n+}:Cu^{2+} = 1:1:1$. L = **4a** (top left), **4b** (bottom left), **5a** (top right), and **5b** (bottom right). Cps = counts per second.

products, 3-(R′)-4,4-di(R′)-8-R-4-bora-3a,4a-diaza-s-indacene (**4a**, R = 2-T, R′ = 2-T; **4b**, R = 3-T, R′ = 2-T; **5a**, R = 2-T, R′ = 3-T; **5b**, R = 3-T, R′ = 3-T; T = thienyl), acquired in modest isolated yields (**4a**, 31%; **4b**, 35%; **5a**, 11%; **5b**, 8.5%) with melting points in the range of 163−184 °C. Compounds **4a**−**5b** were stable as solids or solutes (organic solvents) over a period of several months with no signs of decomposition. The four thienyl groups represent heavy substitution of the BF_2−dipyrrin skeleton, from which a ∼250% increase in molecular weight is attained (Figure 1). Most noteworthy for the present study at hand is that for **4a** and **4b** these groups impart an L_3 neutral [SSS] binding core discussed below. The differences between simple 2- and 3-thienyl positioning at a BF_2−dipyrrin nucleus gives interesting discrete spectroscopic and binding differences.[41]

The crude mixture of the addition reaction involving **3a**,**b** with thienyllithium (Scheme 1, *iv*) contained other minor colored fractions that were neither fully isolated nor even partially characterized. Some of these species are suspected to be products of oxidation. Other species such as the dithienyl and trithienyl species are expected to be present but have neither been isolated nor characterized. They may form predominantly in this same "one-pot" protocol upon control of thienyllithium concentration. Mass spectral data obtained in the form of MALDI-TOF spectra for all ligands (**4a**−**5b**) bore peaks with maximum values of 483.99−484.41 *m/z*, close to the shared calculated (M^+) 484 *m/z* value (see Supporting Information). This helps substantiate the presence of pure products (in terms of the number of substituents) as formulated in Scheme 1. The products exhibit less fluorescence intensity than their parents, and whether this and other diminished properties can be gained back (switched on) under the right conditions using external stimuli in the form of metal cations in solution is the subject of this paper.

2-D NMR Spectroscopic Studies. Due to the laborious chromatographic steps required to achieve ample purification of **4a**−**5b** detailed in the Experimental Section, extensive NMR spectroscopic characterization was undertaken to ensure ligand purity *in solution* and elucidate the crowded aromatic region where peaks for the various differently positioned thienyl groups reside. Thus, we not only obtained one-dimensional ^1H and ^{13}C NMR spectra but also utilized $^1H-^1H$ COSY, $^1H-^1H$ NOESY, $^1H-^{13}C$ HMQC, and $^1H-^{13}C$ HMBC to try to assign all protons and carbons. Herein, we will describe NMR spectral details for **4b** only (for said spectra of **4a**, **5a**, and **5b**, see Supporting Information).

The $^1H-^1H$ COSY spectrum of **4b** clearly includes four sets of three signals involving H_a through H_n as designated in Figure 2. This allows for the initial identification of the outlying two doublets for H_d and H_e belonging to the substituted pyrrolyl group. Then, six different signals for the

Scheme 1. (*i*) General Synthesis of Dipyrromethane (Shown Here for the Thienyl Derivatives) via Acid-Catalyzed Condensation,[32,33,43] (*ii*) Oxidation via DDQ to Dipyrrin,[36,48] (*iii*) $F_3B{\cdot}OEt_2$ Addition To Give BF_2−dipyrrin,[36,49] and (*iv*) Formation of the (Ultimately) Tetrasubstituted Species **4a**−**5b** Described Herein

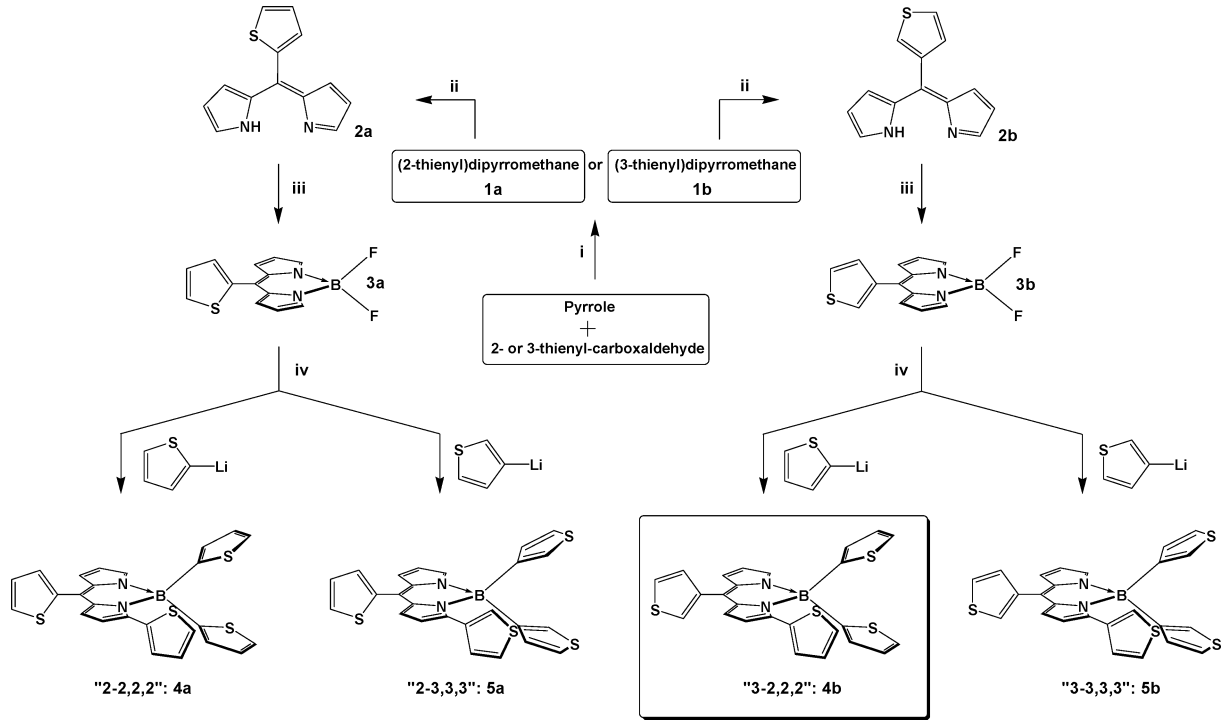

Scheme 2. Proposed Straightforward M^{2+} Binding at the Front Site of **4b** and **5b** ($M = M^{2+}$)

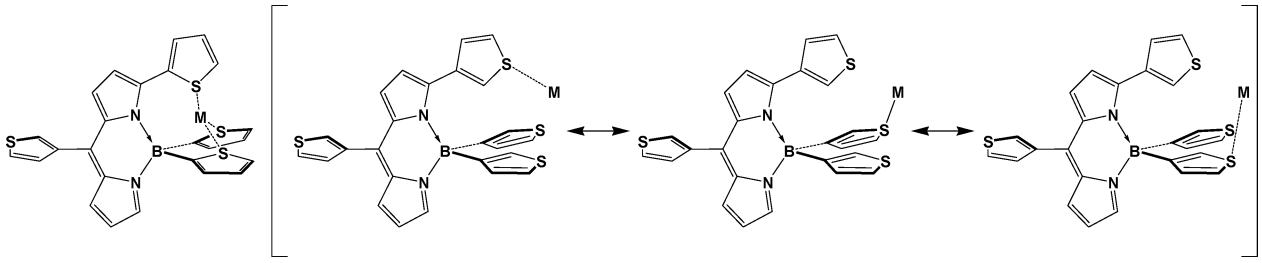

three 2-thienyl groups are found in the respective 2:1 ratios: peaks for H_l, H_m, and H_n are twice as intense as those for H_i, H_j, and H_k. Next, the H_a, H_b, and H_c protons of the sole 3-thienyl group at the 8-position are pinpointed. This leaves H_f, H_g, and H_h to be assigned as the remaining three dipyrrin core protons. Regiochemical assignments among the four trios and the H_d, H_e pair were made via inspecting splitting patterns (Supporting Information) and through the use of $^1H-^1H$ NOESY spectroscopy (Figure 4).

The NOESY contour plot bears five clear cross-peaks: one at ∼7.0, two at ∼7.5, and two at ∼7.8 (Figure 4). Significantly, the encircled peaks are assigned as through-space interactions between H_c-H_d, H_c-H_f, H_b-H_d, H_b-H_f, and H_i-H_l (Figure 4). An interaction is thought to exist between H_e-H_i, but since the signals for H_e and H_i occur together, conformation of its existence is obscured by the heavily marked diagonal.

We further undertook $^1H-^{13}C$ HMQC spectroscopy to assign tertiary carbon signals to their geminal protons (Figures 2 and 5) and $^1H-^{13}C$ HMBC spectroscopy to identify the signals for the quaternary carbon C_1-C_7 (Figures 2 and 6).

Boron NMR spectroscopy, albeit 1-D, is also a useful tool in the characterization of boron−dipyrrins (see Supporting Information). The ^{11}B NMR signals for compounds **4a**−**5b** occurring at δ −3.6 for **4a** and **4b** and δ −3.4 for **5a** and **5b** are marginally diagnostic of the type of thienyl substitution. Notably, the presence of (broad) singlets in place of triplets further confirms the absence of fluorines.

Fundamental UV−Vis Properties of Ligands 4a−5b. First, we can compare the spectral characteristics of the new tetrathiophene derivatives (**4a**−**5b**) to those of parent molecules **3a** and **3b** (Table 1). Generally, the values for λ_{max} possessed by the parent derivatives become red shifted upon such further substitution. Derivative **3a** (505 nm) leads to a λ_{max} value of 563 nm for **4a** and 539 nm for **5a**. Compound **3b** (498 nm) leads to a value of 553 nm for **4b** and 531 nm for **5b**. The values of emission maxima ($\lambda_{em,max}$) result in Stokes' shifts of 25−36 nm. There are also higher energy bands of weaker intensity centered at 397 (**4a**), 370 (**4b**), 386 (**5a**), and 363 nm (**5b**). Extinction coefficients *decrease* moderately from those of the parent **3b** to those of the tetrathienyl species **4b** and **5b**. However, from **3a** to **4a** there is an *increase*, but from **3a** to **5a** there is intensity retention.

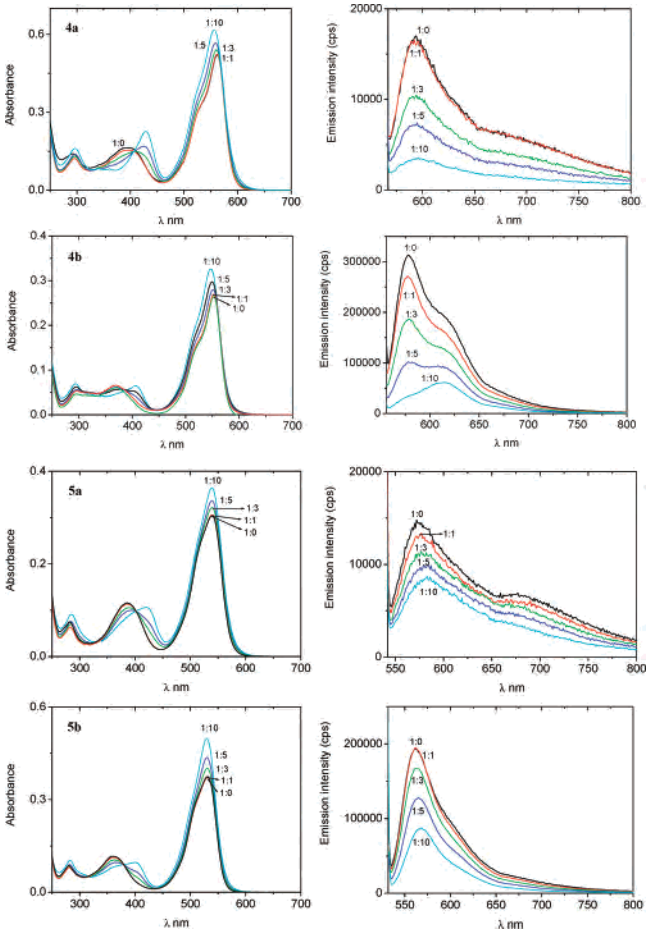

Figure 15. Absorption and emission spectra of **4a** (first row), **4b** (second row), **5a** (third row), and **5b** (fourth row) in CH_3CN. Ligand (**4a**−**5b**) concentration is 1.0×10^{-5} M, and Hg^{2+} additions were made at concentrations of 1.0×10^{-3} M. See Supporting Information for photographs. Excitation wavelengths were as follows: 563 (**4a**), 553 (**4b**), 539 (**5a**), and 531 nm (**5b**).

The ligands exhibit weak fluorescence quantum yields of $\Phi_F = 0.0006-0.012$ (Table 1).

Screening for Metal-Ion Sensing via UV−Vis. Extensive fluorescence and absorption studies were carried out on ligands **4a**−**5b** and are presented and described below. Compounds **4a**−**5b** were screened using various mono- and divalent metal ions. In these trials we used the perchlorate salts of Ca^{2+}, Cs^{+}, Mn^{2+}, Co^{2+}, Cu^{2+}, Ag^{+}, Zn^{2+}, Cd^{2+}, Hg^{2+}, and Pb^{2+}. The most striking feature in these absorption studies was the difference made with Cu^{2+} in the solution of **4b** which gave a rapid and significant diminution upon 1:1 addition with some analogous change also in the case of **4a** (Figure 7). Upon further addition of Cu^{2+}, a rapid (<1 min) color change from pink to clear can be viewed qualitatively with the naked eye under white light (Figure 12). The difference between the signal changes for **4a** and **4b** in Figure 7 is thought to embody an electronic difference at the 8-position between the two isomeric substituents (also see Figure 10). Interestingly, metal ions such as Hg^{2+}, Pb^{2+}, or Ag^{+}, considered to be greatly thiophilic, do not register major differences here.

These differences in the absorption bands for **4b** led us to an investigation of emission characteristics. While the intensity of the absorption band is perturbed the most for **4b**, there are actually fluorescence responses (increases) in the spectra for all ligands (**4a**−**5b**) for Cu^{2+} as shown in Figure 7. These rapid spectroscopic changes shown via UV−vis spectra are also reflected visibly in the photos taken under white light and long UV light (365 nm) (Figure 12). There are now also irregularities upon Hg^{2+} addition where the fluorescence increases for **5b** and slightly for **5a** but decreases for **4b** and slightly for **4a**.

4a−M^{n+} and **4b**−M^{n+} mixtures may involve occupation of the principal binding site, whereas for **5a**−M^{n+} and **5b**−M^{n+} there is no well-defined binding pocket formed by an isolated ligand (Scheme 2). However, intermolecular interaction with the rear thienyl group at the 8-position cannot be precluded and may lead to *non-straightfoward* ligation; this binding would be expected to give rise to a minor (∼25%) effect, owing to the fact that there are four thienyl groups per molecule, unless it promotes internal steric hindrance via an inhibited rotation of the 8-position thienyl group.[34] Our attempts to gauge M^{n+}:ligand complexation appear in the next section.

Binding of Cupric Ion. Since Cu^{2+} gives a signature absorption change, this complex was examined further via titration studies (Figure 9). Notably, a double hump pattern emerges for **4a** and **4b** suggestive of two different species arising from different Cu^{2+} binding modalities. In the spectra for **4a** and **4b** growth of the shoulder (hump on left side centered at 531 nm for **4a** and 522 nm for **4b**) eventually gives way at high Cu^{2+} concentration to a lower energy hump, a band similar to that of the original ligand. Well-defined isosbestic points are present for **4a** at 299 and 423 nm with additional relatively tight ones occurring at 582 and 340 nm. Clear isosbestic points in the absorption spectrum for **4b** are also present at 578 and 475 nm. Likewise, upon bathochromic shifting caused by Cu^{2+} addition isosbestic points 497 and 555 nm are formed in the case of **5a** with counterparts of 465 and 547 nm in the case of **5b**. The Cu^{2+} titration spectra involving **5a** and **5b** retain their general shape but become broad and slightly red shifted upon significant Cu^{2+} addition. Ultimately, all ligands become slightly red shifted upon significant Cu^{2+} addition.

These titrimetric measurements allow us to graph the absorbance changes at $\lambda_{abs,max}$ upon Cu^{2+} addition. In particular, absorbance versus $[Cu^{2+}]/[ligand]$ plots for ligands **4a**−**5b** can be prepared (Figure 10). This graph reveals that **4b** reaches saturation ahead of the others. It can be rationalized from Scheme 2 why **4b** may reach saturation in advance of **5a** and **5b**. Why **4b** reaches saturation before **4a** may be answered in a better understanding of the 8-position thienyl group binding. If **4b** does ligate M^{n+} at the 8-position thienyl, this group will be hindered and likely increase fluorescence as seen for Cu^{2+} but not for Hg^{2+}.

Emission spectra for all ligands in the presence of Cu^{2+} initially increase and then decrease at high concentration, attributed to quenching, common for Cu^{2+} systems.[12] Fluorescence enhancement occurs with a 19-fold increase for **4a**, a 6-fold increase for **4b**, a 3-fold increase for **5a**, and a 2-fold increase for **5b**. These maximum emission intensities upon

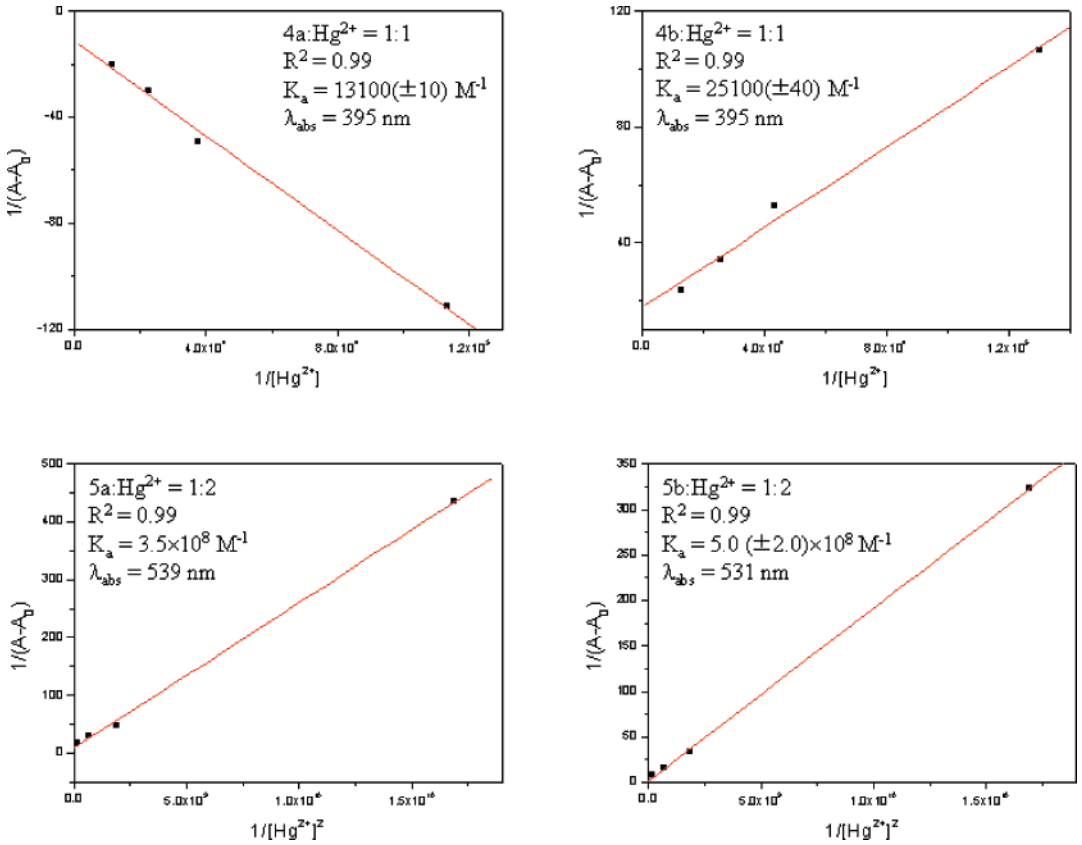

Figure 16. Modeling of ligand−Hg^{2+} binding constants using the Benesi−Hildebrand equations.

Table 3. Selected Bond Lengths (Å) and Angles (deg) for **4b**−**5b**

	4b	**5a**	**5b**
	Bond Lengths (Å)		
B−N(1)	1.572(8)	1.583(7)	1.585(4)
B−N(2)	1.560(9)	1.588(7)	1.588(4)
B−C(41)	1.604(8)	1.614(7)	1.613(5)
B−C(51)	1.618(9)	1.600(7)	1.620(5)
	Angles (deg)		
N(1)−B−N(2)	104.7(5)	104.1(4)	104.4(2)
N(1)−B−C(41)	112.3(5)	109.8(4)	112.4(3)
N(1)−B−C(51)	107.5(5)	111.9(4)	109.5(3)
N(2)−B−C(41)	107.1(5)	107.1(4)	106.5(2)
N(2)−B−C(51)	106.4(5)	107.9(4)	107.5(2)
C(41)−B−C(51)	117.8(5)	115.3(4)	115.7(3)

Cu^{2+} addition were estimated at ligand:Cu^{2+} ratios (followed by μL of Cu^{2+} solution) of ∼1:9, 280 μL (**4a**); ∼1:5, 150 μL (**4b**); ∼1:5, 140 μL (**5a**); and ∼1:4, 120 μL (**5b**). Compounds **4a** and **5b** also engage in noteworthy changes, whereas unpronounced behavior is found for **5a**. These fluorescent patterns are also reflected in photographs of the 4 mL sample vials (Figure 12).

The limit of quantification for Cu^{2+} in the four ligand solutions (1.0×10^{-5} M concentration) is as follows: **4a**−**5b** show detectable responses at 10 μL of Cu^{2+} addition (1.0×10^{-3} M) leading to similar values of [Cu^{2+}] of $\sim 3.3 \times 10^{-6}$ M (270 ppb). For Hg^{2+}, **4a**−**5b** show changes from 20 μL of Hg^{2+} addition giving a [Hg^{2+}] detection limit value of $\sim 6.6 \times 10^{-6}$ M (1.7 ppm). The present naked eye limit of detection for Cu^{2+} in the presence of **4b** in particular is approximately 23 μM, relating to a ligand-to-metal ion ratio of 1:3 as pictured in Figure 12.

To probe binding further we attempted to model the data to extract binding constants for Cu^{2+} using the Benesi−Hildebrand equation.[50] The best agreements using this analysis gave 1:2 M:L binding for the **4**'s and 1:1 binding for the **5**'s: $K_a = 5.0 \pm 0.4 \times 10^8$ M^{-1} (**4a**); $K_a = 1.2 \pm 0.3 \times 10^{10}$ M^{-1} (**4b**); $K_a = 1800 \pm 20$ M^{-1} (**5a**); $K_a = 6200 \pm 30$ M^{-1} (**5b**).

Competition Experiments with Cu^{2+}. We next treated M^{n+}−ligand complexes ($M^{n+} \neq Cu^{2+}$) with cupric ion to gain further insight into complexation and potential photophysical off−on switching behavior upon M^{n+} stimulation. A sample of 1.0 equiv of Cu^{2+} was added to L:M^{n+} mixtures to give a 1:1:1 L:M^{n+}:Cu^{2+} ratio in solution. This treatment affected fluorescence intensity in various ways as shown in Figure 14. The effect Cu^{2+} addition has on the M^{n+}−**4b** systems is particularly pronounced; all mixtures decrease in intensity. Oppositely, for **5b**, fluorescence signals for all L−M^{n+} systems uniformly increase with the greatest increase coming from Ag^+. The general trends for the **5a** systems are similar to those of **5b** with moderate differences for trials involving Mn^{2+}, Ag^+, and Cs^+.

Behavior of Mercuric Ion. The behavior of Hg^{2+}, whose behavior is less pronounced in the context of ligands **4a**−**5b** and their absorbances (Figure 7), was interesting with regard to fluorescence as explored through titration studies, analogous to those done for Cu^{2+}. For the absorption spectra there were minor increases for all four ligands **4a**−**5b**

(50) Benesi, H. A.; Hildebrand, J. H. *J. Am. Chem. Soc.* **1949**, *71*, 2703−2707.

Table 4. HOMO/LUMO Levels for the Geometry-Optimized Structures for **4a**−**5b** (B3LYP/6-31++(G))[a]

	4a	5a	4b	5b
energy (Hartree)	−2689.656229	−2689.645971	−2689.655888	−2689.646352
relative energy (kcal/mol)	0.0	6.4	0.2	6.2
HOMO (Hartree)	−0.21093	−0.21884	−0.21161	−0.21606
LUMO (Hartree)	−0.11570	−0.11707	−0.11291	−0.11293
λ_{max} (nm)	478	448	462	442

[a] 1 Hartree = 627.5094 kcal/mol.

through addition of 10 equiv of M^{n+}. However, the patterns in the emission spectra are opposite: they all systematically degrade as more Hg^{2+} is titrated in, up to 10 equiv. Compound **4b** reveals the greatest change when considering the level of 1.0 equiv addition.

Binding in the case of mercuric ion was modeled using the Benesi−Hildebrand equation (Figure 16).[50,51] The best agreements opposite to those for Cu^{2+} above give 1:1 M^{2+}:L binding for the **4**'s and 1:2 binding for the **5**'s: $K_a = 13\,100 \pm 10\ M^{-1}$ (**4a**), $K_a = 25\,100 \pm 40\ M^{-1}$ (**4b**), $K_a = 3.5 \times 10^8\ M^{-1}$ (**5a**), and ($K_a = 5.0 \pm 2.0 \times 10^8\ M^{-1}$ (**5b**). Binding constant values here for the **4**'s are somewhat pronounced over those for Cu^{2+}.

Binding Reversibility and Direct Cu^{2+}, Hg^{2+} Competition. Separately, we wanted to demonstrate binding reversibility to validate association behavior claimed above. We probed binding reversibility for Cu^{2+} (Figures 25-S, 26-S) and reversibility for Hg^{2+} (Figures 27-S, 28-S) in the case of ligands **4b** and **5b**, respectively, by monitoring immediate absorption changes at room temperature. The results for EDTA complexation with Cu^{2+} in Figures 25-S and 26-S are not convincing: there is a rise in the maximum, but a large baseline distortion also forms; a mild amount of turbidity was observed. The spectra in which ligand−Hg^{2+} mixtures are treated with KI are more convincing (Figures 27-S and 28-S); both maxima return immediately as the **4b** and **5b** ligand systems with 15 equiv of Hg^{2+} are treated with 30 equiv of KI. In these graphs, respective preaddition of EDTA or KI inhibiting complexation is clearly shown.

Separate from the competition supplied in Figure 14 we conducted a binding competition Cu^{2+} and Hg^{2+} for **4b**. With a 1:1 Cu^{2+}:Hg^{2+} presence there is a moderate decrease in absorption signifying that Cu^{2+} forms kinetic products, perhaps owing to the 1:2 ligand-to-metal binding by Cu^{2+} to **4b** (see Figures 29-S−31-S). Upon heating a change in the higher energy band is observed, suggestive of some Hg^{2+} incorporation (Figure 29-S).

Water Addition. By inspection of the complex formulation in Scheme 1 there a clear limitation in water solubility. To test whether our systems as presently substituted exhibit any degree of solubility in water, a relevant solvent in bioprobe analysis, water was premixed with acetonitrile. Hg^{2+} responds similarly with **4b** as before irrespective of water concentration (∼33%), in contrast to the negligible response given by Cu^{2+} in the presence of **4b** (see Figure 32-S, Supporting Information). In fact, responses are minimal for Cu^{2+} for a range of water concentrations (∼20−50% by volume) due perhaps in part to the favorable formation of a Cu^{2+} hydration sphere compared to that formation for Hg^{2+}. In 80% water solutions, however, clusters of red-orange needles precipitate out overnight, leaving a "water"-colored solution. In the cases of the other water solutions (∼20−50%), ligand solubility is maintained for greater than 3 weeks, that is, absolutely no precipitate or solution color change is observed.

X-ray Diffraction Studies. We have undertaken X-ray diffraction studies to (i) further confirm the regiochemistry of thienyl ring positioning as proposed by NMR spectroscopic assignments (Figures 3−6) as well as to (ii) verify geometric considerations of these highly substituted boron−dipyrrins. The molecular structures for **4b**, **5a**, and **5b** were obtained (Figures 17−19), bearing labels for select atoms and featuring all hydrogen atoms. Crystallographic details are provided in Table 2.[52] Notably, these solutions clearly define a chemically sensible boron−dipyrrin frame bearing four pentacyclic heterocycles. A comparison of B−X (X = N, C) bond lengths and bond angles involving the central boron atom is provided in Tables 3 and 4. Curvature of the dipyrrin moiety is present here as mentioned previously.[34,36,53] This puckering is interesting in the context of the [SSS] binding core in which three S's converge toward a point in metal-ion complexation. Further, the 3-position thienyl ring deviates from coplanarity of the attached pyridyl group by ∼29° (**4b**) and ∼56° (**5a**, **5b**) when considering the two mean planes of each pentacycle (non-H atoms only). Changes in geometry are expected to give rise to interesting spectral differences resulting from electronic differences; electronic features of the ligands are discussed below in conjunction with HOMO−LUMO diagrams.

The solutions of **4b** and **5b** involved varying degrees of crystallographic disorder involving the thienyl moieties (see Experimental Section).[36,37,43] This disorder illustrates substituent flexibility, suggestive of facile substituent rotation which may lead to a ligand arrangement that is prepared for metal-ion binding.[54] The NMR spectra reveal signals for all thienyl groups, revealing rotation rapid on the NMR time scale (Figures 3−6; also see Supporting Information). With all this being said, however, there are no previous examples of bisthienyl (2- or 3-) [N_2BC_2] fragments according to the Cambridge Structural Database,[55] underscoring the novelty of **4a**−**5b**.

(51) Saleh, N.; Al-Rawashdeh, N. A. F. *J. Fluoresc.* **2006**, *16*, 487−493.
(52) For bond lengths and angles with esd's, see the Supporting Information.
(53) Montalban, A. G.; Herrera, A. J.; Johannsen, J.; Beck, J.; Godet, T.; Vrettou, M.; White, A. J. P.; Williams, D. J. *Tetrahedron Lett.* **2002**, *43*, 1751−1753.
(54) Chen, J.; Burghart, A.; Derecskei-Kovacs, A.; Burgess, K. *J. Org. Chem.* **2000**, *65*, 2900−2906.
(55) *Cambridge Structural Database*, Version 5.28; Cambidge Crystallographic Data Center: Cambridge, U.K., 2007.

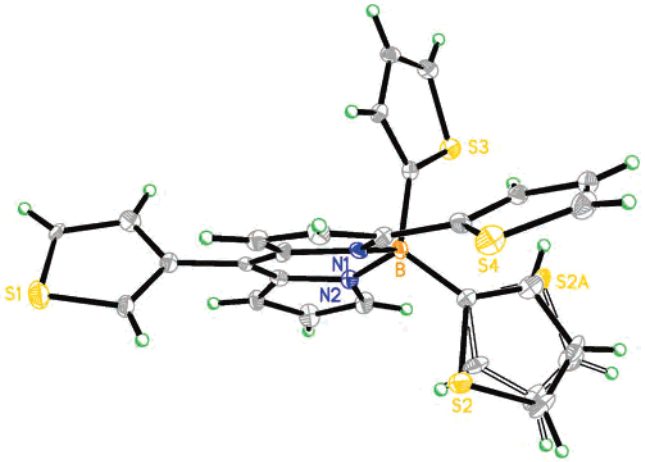

Figure 17. Molecular structure of **4b** (hydrogens are included for completeness).

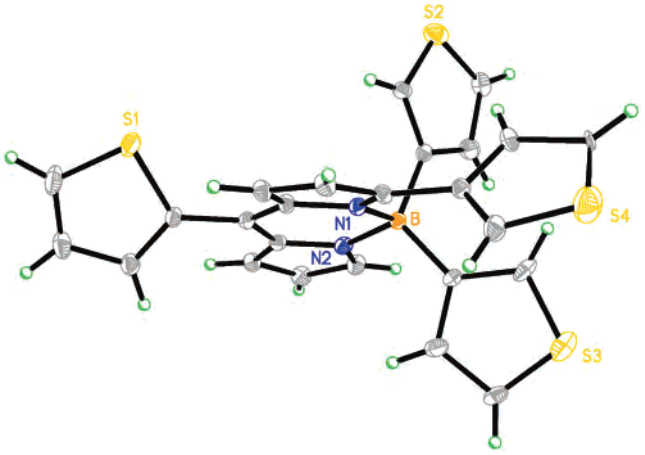

Figure 18. Molecular structure of **5a** (hydrogens are included for completeness).

Molecular structures containing a fragment(s) related to **4b** include principally the [tetrakis(2-thienyl)borate]$^-$. Interestingly, this species does not achieve [Mo(CO)$_3$] complexation, whereas a related neutral S_3 donor, namely, the [tetrakis((methylthio)methyl)borate]$^-$ ion, does. This difference is rationalized by "the magnitude and polarizability of the electronic charge density of the lone pairs on the sulfur atoms."[56] Lone pair density may explain the modest M^{2+} (M = Cu, Hg) binding constants modeled herein for the ligands. Interestingly, this weakened binding may lead to preferable M^{n+} on−off rates that can be explored in further studies.

The binding site in **4a** or **4b** can be further structurally compared to the extremely well-known tris(pyrazolyl)borate system (Tp) system.[57,58] The chelation fragments of the **A**-(Tp), **B**- (B(thienyl)$_4$), and **C**-type (i.e., **4a** or **4b**) each contain three podands composed of hetero-pentacyclic aromatic rings, stemming from a central boron atom either directly or indirectly (Figure 20). The [Tp] **A**-type ligand contrasts with **C** in that **A** is an [N_3], L_2X donor, whereas **C**

(56) Sargent, A. L.; Titus, E. P.; Riordan, C. G.; Rheingold, A. L.; Ge, P. H. *Inorg. Chem.* **1996**, *35*, 7095−7101.
(57) Trofimenko, S. *J. Chem. Educ.* **2005**, *82*, 1715−1720.
(58) Trofimenko, S. *Polyhedron* **2004**, *23*, 197−203.

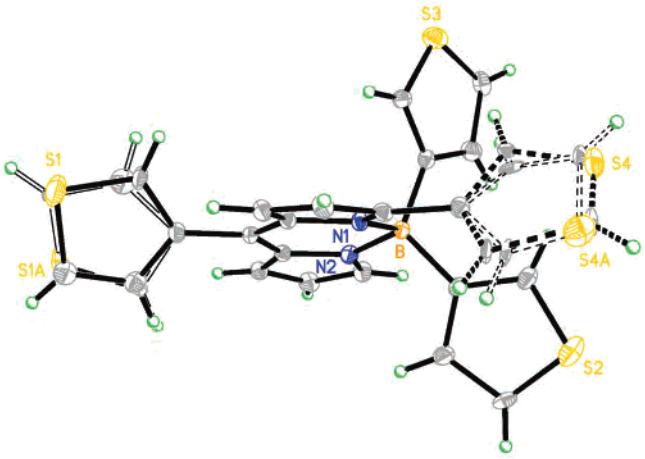

Figure 19. Molecular structure of **5b** (hydrogens are included for completeness).

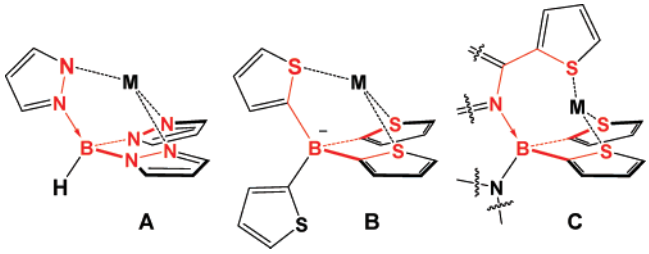

Figure 20. Comparison of three binding cores and their actual or proposed tridentate binding: (**A**) the well-known Tp "scorpionate" core, (**B**) the tetrasubstituted organoborate species,[57,58] and (**C**) the cores for **4a** and **4b**. M = M^{n+}. The ligating core atoms and bonds are in red. L−M bonds are unspecific.[59]

is an [S_3], L_3 donor.[59] The additional two-atom [NC] spacer featured in **C**, and not present in **A**, may provide for some degree of axial ligation character.

Other systems structurally related to **4a**−**5b** but different still from types **A** and **B** include molecules that bear [B(thienyl)$_2$]-type fragments. One report involves derivatives of 8-hydroxyquinolato-based ligands featuring [B(2-benzothienyl)$_2$] units.[60] An ethoxyamine-coordinated fragment also has been reported.[61] Finally, a bipyridine system was reported containing [B(thienyl)$_2$] fragments.[62] These systems involve five-membered boron chelation rings, however, differing by one chelation ring atom with that proposed binding herein for the **4a**−**5b** systems (Figure 2).

Computational Studies. To arrive at a better understanding of the substituent electronic effects of **4a**−**5b**, we undertook density functional theory (DFT) calculations. Note that for all structures in Figure 21 the HOMO state involves a boron−dipyrrin-based HOMO extending onto the thienyl ring at the 3-position regardless of whether this substituent is a 2- or 3-thienyl. 3-Position substituent involvement is also important at the LUMO level (Figure 21). If this thienyl ring becomes statically coplanar, i.e., through M^{n+}−$S_{thienyl}$

(59) Green, M. L. H. *J. Organomet. Chem.* **1995**, *500*, 127−148.
(60) Yi, C.; Liu, Q. D.; Bai, D. R.; Jia, W. L.; Ye, T.; Wang, S. N. *Inorg. Chem.* **2005**, *44*, 601−609.
(61) Low, J. N.; Musgrave, O.; Wardell, J. *Acta Crystallogr., Sect. C* **2000**, *56*, E63−E63.
(62) Weis, N.; Pritzkow, H.; Siebert, W. *Eur. J. Inorg. Chem.* **1999**, 393−398.

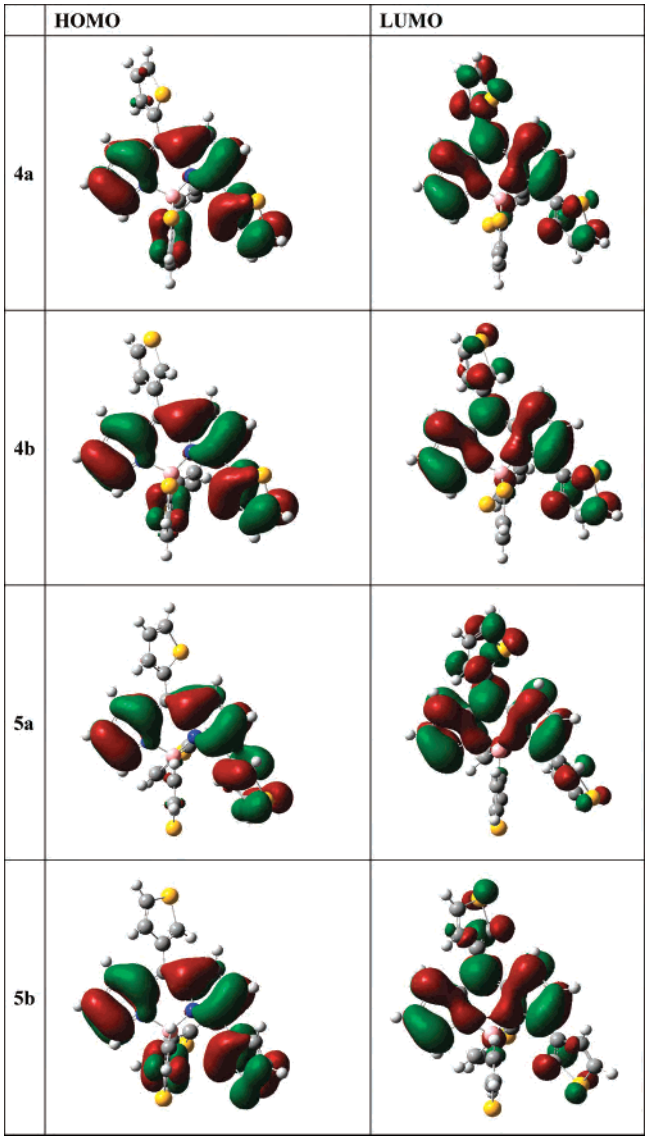

Figure 21. HOMO−LUMO diagrams of geometry-optimized structures of **4a**−**5b** (Gauss View 3.0).

binding, then we may expect greater delocalization over this frame. Further, there is asymmetry with the [B(thienyl)$_2$] moiety for **4a**, **4b**, and **5b**: due to B puckering, one thienyl ring attains an equatorial-like position that lies near the plane, bisecting the boron−dipyrrin core, and bears some amount of electron density, whereas the second thienyl substituent is placed axially and bears little or no electron density in the HOMO.

4. Conclusion

Interest in developing novel sensors and switches that respond to external stimuli, such as metal ions in solution, is driving various research efforts in inorganic and organic chemistry alike. This report is representative of such efforts in trying to style well-defined small-molecule fluorophores into ionophores through rational substitution that gives rise to legitimate receptor sites. Our general strategy is that, with adequate substitution, boron−dipyrrins can serve satisfactorily and in unexpected ways in ionic recognition. We prepared four isomeric tetrathienyl-substituted dipyrrin derivatives as new entries into luminescent organoboron complexes: 3-(R′)-4,4-di(R′)-8-R-4-bora-3a,4a-diaza-s-indacene (**4a**, R = 2-T, R′ = 2-T; **4b**, R = 3-T, R′ = 2-T; **5a**, R = 2-T, R′ = 3-T; **5b**, R = 3-T, R′ = 3-T; T = thienyl). Their existence and high purity are supported by a copious amount of data that includes assorted NMR spectra. Ligand M^{n+} ion hosting tendencies are provided by extensive UV−vis spectroscopic data to give numerous and interesting patterns in M^{n+} recognition. Importantly, upon treatment with metal-ion perchlorate salts (M^{n+} = Ca^{2+}, Cs^{+}, Mn^{2+}, Co^{2+}, Cu^{2+}, Ag^{+}, Zn^{2+}, Cd^{2+}, Hg^{2+}, Pb^{2+}) the solution of **4b** undergoes a rapid pink-to-clear change, visible upon addition of Cu^{2+} with smaller effects seen for **4a**. There was 19-fold fluorescence enhancement seen for **4a**. Upon treatment with Hg^{2+} all ligand solutions show minor absorption increases and significant fluorescence decreases. X-ray diffraction studies and DFT calculations also serve to support our findings. However, we need to engage in further studies to elucidate exact host−guest interactions.

Acknowledgment. D.G.C. gratefully acknowledges financial support from KAIST, KRF, the BK 21 Project, and the Korea Science Academy (Busan, South Korea). We thank Professor Gerard Parkin (Department of Chemistry, Columbia University) for his help in obtaining X-ray diffraction studies of **4b**−**5b**. Hack Soo Shin (KAIST, Department of Chemistry) is gratefully acknowledged for his technical assistance in acquiring *all* NMR spectra. Teresa Lindstead (Cambridge, England) is thanked for her assistance in efficiently depositing our crystallographic data to the CCDC. Professor Hong-ku Shim is acknowledged for the use of his photoluminescence spectrometer. MALDI-TOF were gratefully obtained with the help of the KAIST research supporting team. The reviewers of this manuscript are acknowledged for their many insightful comments.

Supporting Information Available: 1-D ^{1}H and ^{13}C NMR spectra and 2-D COSY, NOESY, HMQC, and HMBC spectra; ^{11}B NMR spectra; UV−vis absorption and emission spectra for **3a** and **3b**; high-resolution MALDI-TOF mass spectra; details of X-ray studies; UV−vis absorption data for binding reversibility and selectivity tests for Hg^{2+} and Cu^{2+} and water-containing solutions. This material is available free of charge via the Internet at http://pubs.acs.org. CIF files of the crystallographic determinations for **4b**−**5b** were deposited with the Cambridge Crystallographic Data center (CCDC), and codes CCDC 641774 (**4b**), 641776 (**5a**), and 641775 (**5b**) were allocated. These data are available without cost at www.ccdc.cam.ac.uk/conts/retrieving.html or from the CCDC, 12 Union Road, Cambridge CB2 IEZ, United Kingdom; fax +44-(0)1223-336033; e-mail: deposit@ccdc.cam.ac.kr.

IC701101J